

Accepted Manuscript

Origin of insoluble organic matter in type 1 and 2 chondrites: new clues, new questions

Eric Quirico, François-Régis Orthous-Daunay, Pierre Beck, Lydie Bonal, Rosario Brunetto, Emmanuel Dartois, Thomas Pino, Gilles Montagnac, Jean-Noël Rouzaud, Cécile Engrand, Jean Duprat

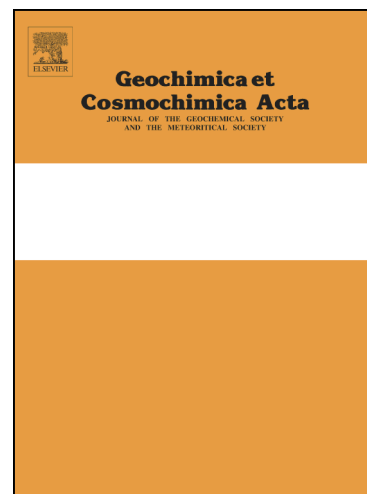
PII: S0016-7037(14)00190-2
DOI: <http://dx.doi.org/10.1016/j.gca.2014.03.025>
Reference: GCA 8732

To appear in: *Geochimica et Cosmochimica Acta*

Received Date: 24 May 2013
Accepted Date: 19 March 2014

Please cite this article as: Quirico, E., Orthous-Daunay, o-R., Beck, P., Bonal, L., Brunetto, R., Dartois, E., Pino, T., Montagnac, G., Rouzaud, J-N., Engrand, C., Duprat, J., Origin of insoluble organic matter in type 1 and 2 chondrites: new clues, new questions, *Geochimica et Cosmochimica Acta* (2014), doi: <http://dx.doi.org/10.1016/j.gca.2014.03.025>

This is a PDF file of an unedited manuscript that has been accepted for publication. As a service to our customers we are providing this early version of the manuscript. The manuscript will undergo copyediting, typesetting, and review of the resulting proof before it is published in its final form. Please note that during the production process errors may be discovered which could affect the content, and all legal disclaimers that apply to the journal pertain.



**ORIGIN OF INSOLUBLE ORGANIC MATTER IN TYPE 1 AND 2 CHONDRITES:
NEW CLUES, NEW QUESTIONS**

Eric Quirico¹, François-Régis Orthous-Daunay^{1#}, Pierre Beck¹, Lydie Bonal¹, Rosario Brunetto², Emmanuel Dartois², Thomas Pino³, Gilles Montagnac⁴, Jean-Noël Rouzaud⁵, Cécile Engrand⁶, Jean Duprat⁶

[1] Institut de Planétologie et d'Astrophysique de Grenoble (IPAG), Université Grenoble Alpes / CNRS-INSU, UMR 5274, Grenoble F-38041, France

[2] Institut d'Astrophysique Spatiale (IAS), Université Paris-Sud, UMR 8617-CNRS INSU, Bât 121, F-91405 Orsay, France

[3] Institut des Sciences Moléculaires d'Orsay (ISMO), UMR 8214-CNRS Université Paris Sud, bât.210, F-91405 Orsay Cedex, France

[4] Laboratoire de Géologie de Lyon, CNRS, Ecole Normale Supérieure de Lyon, 46 allée d'Italie – BP 7000, 69342 Lyon Cedex 07, France

[5] Laboratoire de Géologie de l'Ecole Normale Supérieure, UMR CNRS 8538, 24 rue Lhomond, 75321 Paris Cedex 5, France

[6] Centre de Spectrométrie Nucléaire et de Spectrométrie de Masse (CSNSM), Université Paris-Sud, UMR 8609-CNRS/IN2P3, F-91405 Orsay, France

[#] New address: Laboratory for Space Sciences, Physics Department, Washington University in St. Louis, One Brookings Dr., St. Louis, MO 63130, USA

To whom correspondence should be addressed:

Eric Quirico

E-mail: eric.quirico@obs.ujf-grenoble.fr

Tel 33 4 76 51 41 56

ABSTRACT

Insoluble organic matter (IOM) extracted from primitive chondrites is a polyaromatic solid with a structure and composition resembling that of terrestrial kerogens. A survey of its composition and structure has been carried out on a series of 27 CR, CM, CI and ungrouped C2 carbonaceous chondrites (Tagish Lake, Bells, Essebi, Acfer 094) using infrared and multi-wavelength Raman micro-spectroscopy (244, 514 and 785 nm laser excitations). The results show that chondritic IOM from PCA 91008 (CM2), WIS 91600 (CM2), QUE 93005 (CM2), Tagish Lake (C2 ungrouped) and possibly Cold Bokkeveld (CM2) has been subjected to the past action of short duration thermal metamorphism, presumably triggered by impacts. The IOM in most of the CM chondrites that experienced moderate to heavy aqueous alteration may have been slightly modified by collision-induced heating. However, even IOM from chondrites that escaped significant thermal metamorphism displays Raman characteristics consistent with a formation by thermal processing, either in the protosolar disk or in the parent body. An alternative energetic process to thermal heating is ion irradiation. After thoroughly analyzing both these scenarii, no conclusion can be drawn as to which is the most plausible mechanism nor whether the heating process took place prior or after accretion. The results show for the first time that the width of the G band in spectra collected with a 514 nm excitation correlates with the O/C atomic ratio, suggesting a major role of oxygen in the cross-linking of polyaromatic units.

1. INTRODUCTION

The origin of organic matter (OM) in primitive chondrites has been an ongoing and open debate over the last 40 years. After the discovery of extraterrestrial amino acids in Murchison in the 70s, Fischer-Tropsch reactions in the solar nebula were invoked to account for the formation of both soluble (SOM) and insoluble (IOM) organic matter (Hayatsu et al., 1977). The discovery of high D and ^{15}N enrichments in the 80s led to the idea that chondritic OM was inherited from the interstellar medium (ISM) (Robert and Epstein, 1982; Yang and Epstein, 1983; Cronin and Chang, 1993; Alexander et al., 1998). Indeed, such large fractionations require low temperature chemistry ($< 20\text{ K}$) that could not occur in the warm region of the protosolar disk where asteroids formed. This statement was at that time consistent with the good spectral match of the $3.4\ \mu\text{m}$ band observed in diffuse ISM and in IOM extracted from the Orgueil and Murchison chondrites (Ehrenfreund et al., 1991; Sandford et al., 1995). Nevertheless, the idea soon emerged that organics recovered in chondrites were the result of a long chain of processes (see Kerridge, 1999 for a review). Soluble OM has for instance been considered as the product of precursors that interacted with aqueous fluids in the parent asteroid (Cronin and Chang, 1993).

Mid-infrared observations of diffuse ISM have since shown differences with IOM spectra and consequently the diffuse ISM $3.4\ \mu\text{m}$ band has been re-assigned to amorphous hydrogenated carbons (Pendleton and Allamandola, 2002; Dartois et al., 2004; Dartois et al., 2007). The infrared spectral features expected for the IOM candidate have never been detected in dense molecular clouds. This debate has also evolved greatly since the return of the STARDUST mission sample and the inventory obtained from more than 30 years of extensive analysis of stratospheric Interplanetary Dust Particles (IDPs) and Antarctic micrometeorites (AMMs) (Wopenka et al., 1988; Flynn et al., 2003; Keller et al., 2004; Brownlee et al., 2006; Quirico et al., 2005a; Busemann et al., 2009; Dobrica et al., 2009, 2011). The detection of crystalline minerals in STARDUST grains and the ubiquitous presence of a polyaromatic solid showing strong similarities with chondritic IOM in grains of presumed cometary origin (AMMs and chondritic porous stratospheric IDPs) have challenged the idea of ISM heritage, as these crystalline minerals were definitely formed in the protosolar disk.

Alternative scenarios to ISM inheritance have been proposed over the last 10 years. Cody et al. (2011) suggested that IOM formed from H_2CO polymerization, followed by thermal maturation in the parent body. This study also proposed a common origin of IOM from chondrites and stratospheric IDPs. The observed correlation between the D/H ratio and the binding energy of the C-H bond has been interpreted as evidence of IOM formation in warm and ionizing regions of the protosolar disk, followed by a deuteration process in the upper disk layer (Gourier et al., 2008; Remusat et al., 2006, 2009, 2010). However, these studies do not propose a formation mechanism for IOM. Okumura et al. (2011) suggested that IOM is composed of two distinct components, a D-poor and ^{13}C -poor aromatic fraction and a thermally labile D-rich and ^{13}C -rich aliphatic fraction, both of interstellar origin.

Post-accretional evolution of organic matter has also emerged as a critical issue, as it may disturb or even obscure pre-accretional information. In type 1 and 2 chondrites, evidence of short duration thermal heating of OM has been found using a variety of techniques (Kitajima et al., 2002; Naraoka et al., 2004; Cody and Alexander, 2005; Alexander et al., 2007; Yabuta et al., 2005, 2010; Kebukawa et al., 2010; Orthous-Daunay et al., 2013). Oxidation processes induced by aqueous alteration have been proposed to account for the variation of aliphatic abundances across and within chondrite groups (Cody and Alexander,

2005; Herd et al, 2011). Other studies have concluded that such an effect was negligible in chondrite parent bodies and that chemical variability was controlled by short duration thermal metamorphism and chemical heterogeneity of the accreted precursors (Quirico et al., 2009; Orthous-Daunay et al., 2013).

In the present work, we present a Raman study of a series of 27 type 1 and 2 chondrites, along with new IR measurements that complement those of Orthous-Daunay et al. (2013). Raman measurements were performed using three excitation wavelengths – 244, 514 and 785 nm – to take advantage of the dispersion effect of the carbon bands, which unambiguously characterize the polyaromatic structure (Ferrari and Robertson, 2001). The structure of the most primitive chondritic IOM is compared with the structure of various synthetic and natural terrestrial carbon materials, as well as that of stratospheric IDPs and AMMs. We show that the structure of chondritic IOM is consistent with thermal heating, which possibly occurred in the protosolar disk prior to accretion or within the parent body. In this regard, IOM and SOM would have been produced by carbonization of organic precursors formed either in the protosolar disk or on the presolar dense core.

2. SAMPLES AND ANALYTICAL METHODS

2.1 Samples

We studied a series of 27 chondrites: 23 belonging to the CI, CM and CR groups and 4 ungrouped C2s (Table 1). All these samples experienced varying degrees of post-accretional processes such as aqueous alteration and short duration thermal processing. The CI chondrites in this series are Orgueil, Ivuna and Alais. The CR chondrites are EET 92042, GRA 95229, MET 00426, LAP 04516, MAC 87320, PCA 91082, QUE 99177 and Renazzo (types 2) and GRO 95577 (type 1). The CM2 chondrites are the Antarctic finds QUE 97990, QUE 99355, QUE 93005, PCA 91008, WIS 91600 and the falls Mighei, Cold Bokkeveld, Murchison, Murray and Banten. The two CM2 chondrites PCA 91008 and WIS 91600 are metamorphosed CMs (Wang and Lipschutz, 1998; Yabuta et al., 2010). The ungrouped C2 chondrites are Tagish Lake, Bells, Essebi and Acfer 094. The samples were provided by the Johnson Space Center – NASA (Houston, USA), Smithsonian Museum (Washington), Naturhistorisches Museum (Vienna, Austria) and Museum National d'Histoire Naturelle (Paris, France).

The CI chondrites are the most aqueously altered of the series, with alteration degrees ranking in the order Orgueil > Ivuna >> Alais (Endreß and Bischoff 1996). All the CRs experienced aqueous alteration on their parent bodies with no detectable thermal processing (Abreu and Brearley, 2008, 2010; Bonal et al., 2013). We performed IR spectroscopy on these chondrites, providing a data set that complements the survey of Bonal et al. (2013), indicating that all these objects have a hydrated matrix (Fig. 1). The magnitude of aqueous alteration (GRO 95577 >> Renazzo > other chondrites) can be inferred from the shape of the 3 μ m band, which is controlled by the Mg/Fe ratio of serpentines (Beck et al., 2010). IR spectroscopic measurements were also performed on Banten, PCA 91008, WIS 91600, Bells and Essebi (Fig. 1). PCA 91008 is fully anhydrous with no detectable hydrated minerals, consistent with its thermal history. WIS 91600 is hydrated and similar to other CM2s, with no detectable heating effects in minerals. NMR (Nuclear Magnetic Resonance) measurements on IOM demonstrate the past action of thermal metamorphism on this sample (Yabuta et al., 2010). The extent of this process was either weaker than that on PCA 91008 or occurred during or after aqueous alteration. Banten, Tagish Lake, QUE 93005, Bells and Essebi all exhibit a hydrated matrix that can be interpreted as resulting from moderate (Banten) to large

(others) extents of aqueous alteration. Note however that the total amount of water in the Tagish Lake sample is lower than in unheated CMs according to thermogravimetric measurements (Montes-Hernandez et al., 2013). This may be consistent with a thermal event post-dating fluid circulation. The intensity of aqueous processes in other CMs is indicated by their respective petrologic types (Rubin et al., 2007). Details on IR measurements can be found in sections 2.4 and 4.5.

2.2 Insoluble Organic Matter extraction

The extraction of IOM was performed with a dedicated reactor designed to process micrometric matrix samples (~100 μg) within a short time (~ 36 hours) (Orthous-Daunay et al., 2010). Small matrix fragments were separated from the bulk chondrite under a binocular and deposited on a Teflon grid with a $0.5 \times 0.5 \mu\text{m}^2$ mesh. The grid was placed in the reaction chamber of the reactor, where liquids were simultaneously injected and expelled by a peristaltic pump (typical flow ~ 90 $\mu\text{l s}^{-1}$). A first tank contained the liquids necessary for the operation while a second tank was used for waste. Both tanks and the reaction chamber were maintained in an argon atmosphere during the whole demineralization process. The acid treatment protocol was similar to that currently described in the literature (e.g. Gardinier et al., 2000). In a first step, soluble low molecular weight molecules were removed using polar (methanol) and non-polar (CH_2Cl_2) solvents. Then, carbonates were removed by HCl treatment and silicates by HF/HCl treatment. Finally, entrapped soluble molecules were expelled by further washing with $\text{MeOH}/\text{CH}_2\text{Cl}_2$.

2.3 Raman micro-spectroscopy

Raman micro-spectroscopy was mainly performed at Laboratoire de Géologie de Lyon (LGL: Université Claude Bernard - Ecole Normale Supérieure de Lyon, France). We used a LabRam Raman spectrometer (Horiba Jobin-Yvon) equipped with a 600 gr/mm grating and a Spectra Physics Ar+ laser that provided a 514 nm excitation wavelength. The laser beam was focused through a x100 objective, leading to a ~ 0.9 μm circular spot. The typical power on the sample and acquisition time were 300 μW and 90 s, respectively. Spectra were acquired in the 490-2230 cm^{-1} spectral range. The measurement conditions were kept rigorously constant to improve measurement reproducibility (Quirico et al., 2005b). They were also designed to optimize the intensity of the Raman bands with respect to the fluorescence intensity, thus minimizing spectral perturbations due to baseline subtraction. Additional measurements were performed at SOLEIL (SMIS Beamline) with a DXR Raman spectrometer from Thermo Fisher Scientific with a 532 nm excitation laser and a power on sample less than 0.1 mW. The spectral resolution was 4 cm^{-1} and the spatial resolution about 1–2 μm . Measurements were mostly performed on raw matrix grains to enhance heat dissipation with surrounding minerals. Indeed, IOM from type 1 and 2 chondrites appear to be very sensitive to laser irradiation.

Raman spectroscopy using UV excitation was performed with a HORIBA Jobin Yvon LabRam system with a frequency-doubled Ar+ (244 nm) excitation and a 40 \times objective, located at the Laboratoire de Géologie de Lyon (France). The width of the illuminated sample area was 4–5 micrometers. A 600 g/mm spectrometer grating was used in the UV Raman study. The laser power delivered to the sample was limited to 100–500 μW to avoid damage by the incident beam (Quirico et al., 2008).

Raman measurements with 785 nm excitation were performed with a InVia Renishaw microprobe at Laboratoire de Géologie at Ecole Normale Supérieure de Paris (France). The spectra were collected under a microscope (50 \times objective) and circular polarization of the

excitation laser was used. The Raman-scattered light was dispersed by a holographic grating with 1800 lines/mm and detected by a charge coupled device (CCD) camera. Very low incident power was used to avoid local heating.

For both 785 and 244 nm excitations, measurements were mostly performed on IOM samples. Measurements on raw matrix grains generally led to spectra of poor quality with low signal-to-noise ratios. We however checked that measurements on IOM and raw matrix grains provide fairly consistent results.

2.4 Infrared microscopy

Infrared spectra were obtained with a Bruker Hyperion 3000 infrared microscope at IPAG (Grenoble - France). The IR beam was focused through a x15 objective and the typical size of the spot on the sample was $50 \times 50 \mu\text{m}^2$. Spectra were measured at 4 cm^{-1} spectral resolution with an MCT detector cooled with liquid nitrogen. The spectral range was $4000\text{-}650 \text{ cm}^{-1}$. Particular care was devoted to sample preparation, a critical issue in infrared microspectroscopy. Samples must be thin ($< \sim 1 \mu\text{m}$) and their surface sufficiently flat to avoid absorption band saturation and scattering artifacts, respectively (Raynal et al., 2000). IOM grains (typical size $\sim 50 \mu\text{m}$) were picked off the Teflon filter and transferred onto a $3 \times 0.5 \text{ mm}$ diamond window (type IIa synthetic diamond). These operations were performed under a binocular microscope in a class 100 laminar flow hood using a brush bristle or a tungsten needle. The grains were then crushed by applying another diamond window, and the window containing the most crushed grains with an optimal shape was selected. It was placed in an environmental cell equipped with turbomolecular and primary pumps (typical vacuum $\sim 10^{-6}$ mbars). Measurements on IOM grains were performed at $50 \text{ }^\circ\text{C}$. Use of an environmental cell ensured the absence of adsorbed water on IOM samples. A similar procedure was used to prepare raw matrix grains, which were previously separated from chondrules and opaque minerals under the binocular microscope. Samples were gradually heated up to $300 \text{ }^\circ\text{C}$ with spectra recorded during pauses at 100 , 150 and $200 \text{ }^\circ\text{C}$. This procedure made it possible to identify the different types of water molecules or hydroxyl groups trapped within matrix minerals (Beck et al, 2010). Complementary measurements were performed on KBr pellets (1 mg of raw matrix; 300 mg KBr) that were heated a few seconds at $300 \text{ }^\circ\text{C}$ to remove adsorbed water. They provided access to the 10 and $20 \mu\text{m}$ bands related to the stretching and bending modes of SiO_4^{4-} .

3. ANALYTICAL TREATMENT OF RAMAN SPECTRA

Analytical treatment is the cornerstone of a reliable analysis of disordered carbonaceous solid Raman spectra. The 514 nm Raman spectra of most type 1 and 2 chondrites consist of broad first-order carbon bands (the so-called G and D bands or peaks) superimposed on a fluorescence background of variable intensity (Fig. 2). Across the series of chondrites, spectral variations are weak and easily masked by fluctuations of the fluorescence background. For this reason, a multi-step analytical procedure is applied. The first step is the extraction of the Raman bands by subtracting the fluorescence background, assuming a linear shape within the $800\text{-}2000 \text{ cm}^{-1}$ range. However, the baseline is most likely not strictly linear and there is no reliable method to accurately determine its actual shape. Therefore spectra exhibiting the highest Raman/fluorescence ratios and good signal-to-noise ratios were selected by visual analysis. We then applied a so-called Lorentzian-Breit-Wigner-Fano

(LBWF) fit to the selected spectra (see details below). Raman spectral parameters such as width at half maximum (FWHM-G, FWHM-D), peak position (ω , ω_D) and ratio of peak intensity (I_D/I_G) of the G and D bands were then obtained. For each parameter, this treatment revealed a main cluster of spectra and isolated spectra with physically unrealistic values that were considered to be blurred by fluorescence. We finally selected 422 out of the 734 spectra recorded at ENS-Lyon with a 514 nm excitation. The peak intensity of the G band was set to 1 in order to normalize the whole set of data. The second step is the extraction of the spectral information contained in the first-order carbon bands. For this, we applied a Lorentzian Breit-Wigner-Fano (LBWF) fit (Ferrari and Robertson, 2000; Fig. 3). This model was used for a number of reasons. Part of this study involves comparison with the results of Ferrari and Robertson (2001) obtained with a LBWF fit. Because of the sensitivity of the Raman parameters to the curve-fitting model, we had to use the same model. Moreover, we observed that the LBWF fit provides a better correlation with parameters extracted from raw spectra than other fits, especially for the I_D/I_G parameter (Fig. 4). We also used principal component analysis as a complementary method. We observed that the parameters derived from the LBWF fit correlate fairly with the projection of the spectra along the 3 first principal components (Fig. 5).

Several methods for treating Raman spectra can be found in the literature. They are based on various curve-fitting models or principle component analysis. We emphasize that the first-order carbon bands are a vibrational density of states convolved by the absorption coefficient of the material, resulting in a complex Raman continuum that cannot be physically interpreted with a simple curve-fitting model (Ferrari and Robertson, 2000). In this respect, the curve-fitting models currently used in the literature are phenomenological decompositions used to quantify spectral variations from one spectrum to another. Principal component analysis accounts for all spectral variations of the Raman spectra with a high degree of accuracy. However, the final results depend on the data set itself and cannot be compared with results from another study.

The Raman spectra obtained with a 244 nm excitation exhibit no fluorescence background. They were also fitted with an LBWF model, but no principal component analysis was performed given the small number of spectra. The Raman spectra obtained with a 785 nm excitation have an intense fluorescence background, with a curve that is not monotonic. In this case we simply extracted the G-band peak position from the raw spectra. Finally, thanks to data measured with 3 different excitation wavelengths, we calculated the dispersion of the G-band peak position (Ferrari and Robertson, 2001).

4. RESULTS

4.1 514 nm Raman measurements

Most of the spectra show broad G and D bands superimposed on a fluorescence background (Fig. 2). Exceptions are PCA 91008 and WIS 91600, characterized by a very weak fluorescence background. The intensity of the fluorescence background in Tagish Lake varies from moderate to high. No data were collected on raw matrix grains from the three CI chondrites due to an extremely high fluorescence background, which is presumably induced by a process similar to so-called *concentration quenching* (Bertrand et al. 1986). *Concentration quenching* is a process that accounts for the variation of fluorescence intensity upon fluorophores concentration: in a first step fluorescence increases, and in a second step it decreases above a threshold due to reabsorption of fluorescence by the fluorophores. Here,

size, size distribution and concentration of IOM particles within matrix are controlled by the extent of aqueous alteration and we infer these characteristics are significantly different in Orgueil than in type 2 chondrites. This likely leads to variable fluorescence intensity (Le Guillou et al., in press).

LBWF fitting and principal component analysis account for weak variations of the shape, intensity, width and peak position of the G and D bands (Fig. 6). The FWHM-D versus I_D/I_G diagram (Fig. 6a; Table 2) reveals a main group containing most of the studied chondrites (this main group is composed of both the blue and orange groups), except Acfer 094 and PCA 91008 that plot apart from this main group with higher FWHM-D and I_D/I_G . The dispersion of the Raman parameters in PCA 91008 is the largest of the whole data set and is consistent with the spectral variability observed by the naked eye. Within the main group, CMs tend to plot apart from CRs with a larger FWHM-D. The ungrouped WIS 91600, Tagish Lake, Bells, GRA 95229 and Essebi chondrites have smaller I_D/I_G and larger FWHM-D parameters (orange group in Figure 5) than most of other chondrites (blue group, note that QUE 93005 and Cold Bokkeveld are quite close to the orange group).

In the FWHM-G versus ω diagram (Fig. 6b), we observe a main group containing most CM and CR chondrites, WIS 91600 and Tagish Lake (note the two latter chondrites belong to the orange group in Figure 6a). CRs and CMs possibly define two subgroups that overlap, CM chondrites having higher FWHM-G and lower ω than CRs. QUE 93005 exhibits the lowest FWHM-G (around 80 cm^{-1}) and highest ω and is apart from the others. PCA 91008 also plots apart, as well as Bells, Essebi and GRA 95229. ω distinguishes a main group from PCA 91008, WIS 91600, Cold Bokkeveld and to a lesser extent WIS 91600.

Principle component analysis provides results (Fig. 7) that are consistent with those of spectral analysis, except for the lack of distinction of Cold Bokkeveld. It also points to possible differences of Nogoya and QUE 99355 with respect to other CMs, which did not appear with LBWF fitting. In the following, we will consider spectral differences indicated by both LBWF fitting and principle component analysis to be reliable. Therefore, Cold Bokkeveld, Nogoya and QUE 99355 are considered to belong to the main group of chondrites.

Raman spectra are very sensitive to experimental conditions. In this respect, the comparison with earlier results can be achieved only for series of chondrites, as Raman parameters exhibit a systematic shift depending on the experimental conditions (Quirico et al. 2005b). We compared the trends of Raman parameters FWHM-G, FWHM-D and I_D/I_G with those obtained by Busemann et al. (2007) for EET 92042, GRA 95229, GRO 95577, Mighei, Murray, Cold Bokkeveld, Bells and Tagish Lake (Fig. 8). We found no correlation. In contrast, Quirico et al. (2011) observed a very good linear correlation of FWHM-D values from their own data with those from Busemann et al. (2007) and Bonal et al. (2006, 2007) on type 3 chondrites. In the present study, we directly measured the structure of IOM in raw matrix grains. The presence of minerals clearly helped dissipate heat during laser irradiation. In contrast, Busemann et al. (2007) made measurements on pure IOM grains extracted from raw rocks by HF/HCl acid treatments, which were more sensitive to laser heating. Sample sensitivity to laser irradiation may then be a factor accounting for differences between the two data sets. A second factor that may be involved is the fluorescence background, for which spectral subtraction was carried out assuming a linear baseline in both our study and that of Busemann et al. (2007). As mentioned before, the fluorescence background is likely non-linear. The baseline correction therefore may have induced fluctuations in the Raman parameters of the G and D bands. Furthermore, note that Busemann et al. (2007) used a free-

floating baseline, as opposed to us. We performed several tests that show that the final parameters are sensitive to this choice. It is finally difficult to decipher the respective contribution of both these factors, as all IOMs from type 1 and 2 chondrites are both fluorescent and sensitive to laser irradiation. Busemann et al. (2007) report very small errors of the mean for each Raman parameter (e.g. $\sim 0.1 \text{ cm}^{-1}$ for FWHM-G). This appears somewhat inconsistent with the much larger variations of the mean across different IOM samples extracted from the same meteorite (e.g. up to 25 cm^{-1} for FWHM-G). In the present study, we recorded far fewer spectra, but we found parameters with much greater dispersion. In this respect, we considered that many chondrites could not be distinguished from one another, in particular in the main groups discussed above (Fig. 6).

Nevertheless, in the present study, FWHM-G correlates linearly with the O/C atomic ratio of IOM (O/C from Alexander et al. 2007), but not with H/C (Fig. 9). This correlation is striking because Raman spectroscopy is not directly sensitive to composition. This may suggest that oxygen has an influence on the sp^2 structure due to a specific speciation. The speciation of oxygen in chondritic IOM is a matter of debate. Nuclear Magnetic Resonance measurements by Cody et al. (2002) first suggested that most of the oxygen was located in carboxylic groups and ketones. However, Cody et al. (2011) revisited this issue and proposed that most of the oxygen was present as furans. Further measurements by independent research groups would be required to obtain firm conclusions. Furthermore, regarding uncertainties on NMR measurements, we cannot exclude that most of the oxygen atoms may be directly implied through ether bridges, which have also been identified in previous studies (e.g. Remusat et al. 2005b). Both ether bridges and furans may influence the vibrational and electronic states of the polyaromatic units, whereas the influence of carbonyl or hydroxyl functional groups should be much weaker. Our observation supports a lower abundance of the latter in all cases.

As already mentioned, raw rock measurements could not be made on CI chondrites due to the high fluorescence background. Therefore, we performed measurements on IOM grains extracted by acid treatment from Orgueil, Murchison and GRA 95229, under highly controlled conditions regarding heating sensitivity to laser irradiation of type 1 and 2 IOM. These grains were measured independently by two operators (RB and EQ), with different Raman spectrometers (Laboratoire de Géologie de Lyon and SOLEIL-Saclay). The measurements confirmed the low I_D/I_G and large FWHM-G of GRA 95229 with respect to other chondrites and revealed that the Raman spectra of Murchison and Orgueil are fairly similar.

4.2 244 nm and 785 nm Raman measurements

Raman spectra acquired with a UV 244 nm excitation are characterized by weak fluorescence, a weak D band and a narrow intense G band (Fig. 10). Naked eye observations show structural heterogeneity at the micrometric scale for PCA 91008. LBWF fits reveal weak spectral variations (Fig. 11; Table 3). In a FWHM-G versus α diagram, Murchison, Cold Bokkeveld, Alais and Orgueil form a “main group” and Tagish Lake, PCA 91008 and WIS 91600 plot apart. In a FWHM-D versus I_D/I_G diagram, Cold Bokkeveld plots apart from the “main group” Orgueil-Alais-Murchison. α values distinguish a main group with PCA 91008 and WIS 91600 that are apart (Table 3). These results confirm the distinct structures of PCA 91008, WIS 91600 and Tagish Lake. They also suggest that IOMs from Murchison, Orgueil and Alais are fairly similar from a structural viewpoint.

The spectra measured with a red 785 nm excitation exhibit extremely high fluorescence and a non-monotonically increasing background (Fig. 12). Exceptions are PCA 91008 and WIS 91600. We extracted the peak position of the G band from these spectra and calculated the α dispersion (cm^{-1}/nm) using data obtained at 514 and 244 nm wavelengths (Table 4).

4.3 IR measurements on IOM

IR measurements were performed on IOM extracted from QUE 93005, WIS 91600, Mighei, PCA 91082, MET 00426 and GRA 95229 to complement the data set from Orthous-Daunay et al. (2013). The spectra consist of vibrational bands superimposed on a spectral continuum, resulting from broad electronic absorption and scattering. The intensity and shape of this background is variable from one chondrite to another. Despite optimized sample preparation, i.e. a planar sample, in some cases scattering was so high that no measurement was possible. We observed that scattering was weaker for IOM samples produced by a standard extraction method (e.g. Gardinier et al., 2000). We infer that the extraction protocol we used tends to lower the abundance of IOM with respect to insoluble minerals (sulfides, oxides) and thus to enhance scattering. Another explanation is that, due to the absence of a grinding stage, a fraction of the remaining minerals in residues may have sizes above 1 μm and therefore be efficient scattering centers for infrared radiation. The spectral continuum was subtracted by calculating a synthetic baseline as a combination of polynomials and sinusoids (Orthous-Daunay et al., 2013).

The corrected spectra display a series of vibrational bands (Fig. 13). The broad feature peaking around 3300 cm^{-1} is assigned to organic hydroxyl groups (carboxylic acid, alcohol) with a possible contribution of adsorbed atmospheric water that could not be fully expelled in the environmental cell. Hydrated sulfates, as secondary products of sulfide oxidation, may also contribute to this feature (e.g. WIS 91600). The structured feature between $\sim 2800\text{-}3000\text{ cm}^{-1}$ is assigned to symmetric and antisymmetric stretching vibrational modes of the methylene (CH_2) and methyl (CH_3) functional groups, with a possible contribution of tertiary CH. The large area ranging between 1800 down to 900 cm^{-1} is the contribution of several functional groups. Carbonyl ($\text{C}=\text{O}$) and $\text{C}=\text{C}$ stretching modes peak respectively at ~ 1700 and 1600 cm^{-1} . The bands peaking at ~ 1450 and 1380 cm^{-1} are assigned to CH_2/CH_3 bending and CH_3 wagging mode, respectively. The broad feature that peaks at $\sim 1200\text{ cm}^{-1}$ (excluding the alkyl modes) is presumably due to C-C skeletal vibrations of aliphatic and aromatic groups, C-O stretching of ether and alcohol groups and C-OH deformation of alcohol. The feature observed at $\sim 1100\text{ cm}^{-1}$ and which is variable from one IOM to another could be due to the stretching vibrational mode of SO_4^{2-} ions in neoformed sulfates. Each spectral feature in the spectra was fitted with Gaussian components. The structure between $2800\text{-}3000\text{ cm}^{-1}$ was fitted by 5 Gaussians with equal FWHM, accounting for the asymmetric (~ 2925 and 2960 cm^{-1}) and symmetric stretching modes of CH_2 and CH_3 (~ 2850 and 2870 cm^{-1}), respectively. The fifth component peaking around 2900 cm^{-1} can be due to the CH functional group or a Fermi resonance (Dartois et al., 2007). These results provided an indication of (i) the alkyl abundance (sum of the integrated absorbance of the five Gaussians) and (ii) the CH_2/CH_3 ratio (ratio of the integrated absorbance of the Gaussian components due to the antistretching modes of CH_2 and CH_3). The ratio of the carbonyl band to the $\text{C}=\text{C}$ band (each fitted by a single Gaussian profile) provided the $\text{C}=\text{O}$ abundance. The results are plotted in Figure 14, along with the data from Orthous-Daunay et al. (2013). Three groups are typically observed. Group I contain chondrites with CH_3 -rich, alkyl-rich and $\text{C}=\text{O}$ -rich IOM. Group II contains

chondrites with alkyl-poor IOM, with the exception of QUE 93005 that has a very high alkyl abundance. The C=O abundance is variable. Group III contains CM chondrites for which the IOM has a low CH₃ abundance and a slightly lower C=O abundance.

4.5 Hydration state of matrices

The hydration degree of matrices was characterized by IR microscopy and IR spectroscopy on KBr pellets heated to 300 °C (Beck et al., 2010). The measurements confirm that all the matrices from CR chondrites are hydrated, as pointed out by Bonal et al. (2013). All the CR2s from the present study have a hydration degree lower than Renazzo, while GRO 95577 (CR1) has an IR spectrum typical of a heavily hydrated matrix, similar to a CI (Fig. 1). The measurements confirm the 2.0 type of QUE 93005 determined by Rubin et al., (2007). Tagish Lake presents an unusual 3 μm band with two bumps, proving the presence of Mg-rich serpentines and strong aqueous alteration. Last, Banten is a poorly altered chondrite. We estimate its petrologic type to be > 2.5.

The peak position of the 3 μm band of Essebi and Bells suggests that they have experienced heavy aqueous alteration. This however disagrees with recent studies that quantified bulk water abundance and concluded that both these meteorites experienced low degrees of aqueous alteration (Alexander et al., 2012; Alexander et al., 2013). This also disagrees with the structure of the 10 μm band (SiO stretching) and the integrated absorbance of the 3 μm band, which both suggest low degrees of aqueous alteration (Beck et al., in press). Different explanations can account for these discrepancies. First, micro-IR measurements may not be representative of the bulk and Bells and Essebi may have larger heterogeneities than CM and CI, for which the method of Beck et al. (2010) was found to be suitable. Second, the mineralogy of Bells and Essebi matrices may be very different from that of CM, CI and CR. This may result from complex asteroidal settings. In our opinion, we cannot draw conclusions without proceeding with further petrological and matrix characterization of Bells and Essebi. Within the scope of the present study, we consider that the post-accretional history of both these chondrites is unclear.

5. DISCUSSION

5.1 Formation of IOM by thermal processing?

We follow here the framework defined by Ferrari and Robertson (2000, 2001), reporting measurements with multiple excitation wavelengths on series of various synthetic carbon films with large structural and compositional diversities. As the first-order carbon bands are dispersive (i.e. their intensity, width and peak positions depend on the excitation wavelength), different excitation wavelengths probe different fractions of the material. Samples that are structurally different may then exhibit similar spectra at a given wavelength and different spectra at another wavelength. Along with the data of Ferrari and Robertson (2001), we use data collected on coal samples (Quirico et al., 2003, 2005b, 2009), irradiated soots (Brunetto et al., 2009), irradiated ices (Strazzula et al., 2001), stratospheric IDPs (Quirico et al., 2005a; Busemann et al., 2009) and Antarctic micro-meteorites (Dobrica et al., 2011).

Comparison of the spectral parameters α , FWHM-G, I_D/I_G (514 nm excitation) and α dispersion reveals that the extraterrestrial IOM samples are basically different from most of

the synthetic carbon films studied by Ferrari and Robertson (2001) (Fig. 15). Only two samples present Raman parameters fairly similar to IOM: hydrogenated tetrahedral (sp^3 -rich) carbon films (ta-C:H) annealed at 600 and 1000 °C (respectively $\omega \sim 1590 \text{ cm}^{-1}$, FWHM-G $\sim 130 \text{ cm}^{-1}$ and $I_D/I_G \sim 0.7$ -1.7). The dispersion of the G-band position ω (~ 0.01 -0.04 cm^{-1}/nm) estimated from 244, 514 and 785 nm excitations confirms this result (Table 4). The Raman parameters of IOM are also fairly similar to those of low rank coals, which experienced low temperature and long duration heating under natural conditions (Fig. 15). Annealed ta-C:H, low rank coals and chondritic IOM are chemically distinct. Annealed ta-C:H contains no oxygen, unlike IOM and coals, and aromatic units are more cross-linked in IOM than in coals (Cody et al., 2002; Cody and Alexander, 2005; Remusat et al. 2005a,b; Derenne and Robert, 2010). These differences result in subtle variations of shape and peak positions of the first-order carbon bands in 514 and 244 nm Raman spectra (Quirico et al., 2009). However, these materials show strong similarities in their polyaromatic structure (nanometer-sized polyaromatic structural units; e.g. Derenne et al., 2005), and their Raman characteristics are fairly similar. From this viewpoint, we will describe them as *structurally fairly similar*.

One way to make analogs relevant to IOM is then to anneal carbon precursors, using a heating episode that can either be short (laboratory timescale) or long (geological conditions). However, a question remains concerning the place where the heating process occurred under natural conditions. The major forms of carbonaceous matter in ISM are hydrogenated amorphous carbon (Sandford et al., 1995) and PAHs (Desert et al., 1990). These compounds are not observed in IOM. The Raman signatures of the more relevant a-C:H analogs (the so-called polymeric type, see Ferrari et al., 2001) are not similar to that of IOM (Dartois et al. 2007) and the PAHs in ISM are much larger than a few rings as observed in IOM (Derenne et al., 2005). Furthermore, the typical 3.4 μm structure observed in diffuse ISM is not detected in molecular clouds, suggesting a dehydration process in the translucent regions of ISM (Godard et al., 2011). Finally, no thermal sequence is expected in the chemical evolution pathway of a molecular cloud toward a dense core. Heating of interstellar material is expected to occur only once the protostar is active. *In this respect, IOM formation by thermal processing would have been possible in the Early solar system from precursors either formed in the presolar molecular cloud, dense prestellar core or the protosolar disk. The place where this thermal processing occurred could have been either the protosolar disk before the accretion of chondrite parent bodies or within the parent bodies.*

5.2 Post-accretional thermal metamorphism induced by impacts

We examine now the issue of IOM formation through parent body thermal metamorphism. Evidence of thermal metamorphism can be obtained from the composition and polyaromatic structure of IOM (e.g. Alexander et al., 2007; Le Guillou et al., 2012). The FWHM-D versus I_D/I_G diagram (514 nm excitation) allows ranking of the degree of thermal metamorphism in type 3 chondrites (e.g. Bonal et al., 2006). We observe here (Fig. 6) that PCA 91008 (CM) and Acfer 094 plot apart the main group, as is the case for Acfer 094. Acfer 094 is a find that experienced terrestrial weathering and its IOM has probably been altered through oxidation processes on the terrestrial ground, as observed for several weathered Saharian chondrites by Alexander et al. (2007). PCA 91008 has a smaller FWHM-D, a higher I_D/I_G and the raw spectra are devoid of fluorescence as usually observed in type 3 chondrites. The peak position and width of the G-band, ω and FWHM-G, as well as the peak position of the D-band ω , are not consistent with a type 3 chondrite (e.g. Bonal et al., 2007). PCA 91008 contains abundant oxides and no hydrated minerals according to IR spectroscopy, consistent

with a parent body heating process subsequent to aqueous alteration (Wang and Lipschutz, 1998; Beck et al., 2012). The low CH_3/CH_2 ratio and low alkyl and carbonyl contents in IOM are consistent with a heating process (Orthous-Daunay et al., 2013). Finally, mineralogical composition and the structure and composition of IOM all point to a rapid post-accretional heating distinct from a long duration thermal metamorphism of radiogenic origin (Orthous-Daunay et al., 2013). This high temperature, short duration process presumably results from impacts.

IOM from WIS 91600 and Tagish Lake presents structural differences with thermally unprocessed chondrites, which appear in the 244 nm Raman data (Fig. 10). Both these chondrites have a hydrated matrix and their water content is fairly similar or slightly lower than in unheated CM chondrites (Garenne et al., 2012; Montes-Hernandez et al., 2013). IR spectra point to a large extent of aqueous alteration that led to a high abundance of Mg-rich serpentines (Beck et al., 2010). Yabuta et al. (2010) have identified two distinct organic domains in WIS 91600 IOM, corresponding to different degrees of condensation of aromatic units. They concluded that WIS 91600 experienced a short duration thermal process on its parent body triggered by impact. They also pointed out similarities with Tagish Lake but favored for a low temperature oxidation process for the latter, implying Fenton reactions (Cody and Alexander 2005), to account for its low alkyl content. Orthous-Daunay et al. (2013) have provided evidence that such a chemical process was unlikely to occur, a statement that is confirmed by the present study (see below). Indeed, the results presented here show that both Raman and IR data for IOM in WIS 91600 and Tagish Lake are similar, indicating a similar structure and composition. The IR data indicate comparable alkyl, CH_3 and $\text{C}=\text{O}$ abundances in these two meteorites, consistent with their comparable H/C ratio (Alexander et al., 2007). The most straightforward explanation is that the Tagish Lake sample we analyzed, with IOM of similar chemical composition to that measured by Alexander et al. (2007), has experienced a short duration heating on the parent body. The large hydration of both WIS 91600 and Tagish Lake may be due to the fact that the impact occurred before the completion of fluid circulation or that the impact was not large enough to entirely dehydrate the host rock.

IOM from QUE 93005 also has a structure different from unprocessed primitive chondrites. The width of the G band is the lowest of the data set, while its peak is the highest (Fig. 6). The composition of QUE 93005 IOM is particularly intriguing. The CH_3/CH_2 ratio and carbonyl contents are both low, whereas the alkyl abundance is larger by a factor of 2 compared to other chondrites. Both low CH_3 and $\text{C}=\text{O}$ contents are not consistent with an unprocessed material in the parent body and point to thermal processing on the parent body. However, thermal processing may appear to be inconsistent with the high alkyl abundance. In fact, it seems that under certain conditions, it is possible to create new alkyl functions, for instance by carbonizing Soluble Organic Matter (SOM), i.e. transforming SOM into IOM. Further shock and heating experiments should be performed to help answer this question (Beck et al., 2011). Cold Bokkeveld is also an intriguing object, with low alkyl content and CH_3/CH_2 ratio, but a $\text{C}=\text{O}$ content similar to that of unprocessed chondrites. The structure of its IOM is fairly similar to that of those chondrites, however some subtle variations have been observed in the 244 nm Raman parameters (Fig. 11).

All CMs except Murchison have a low CH_3/CH_2 ratio, but their polyaromatic structures exhibit no differences with those of CRs or CIs. The effect of aqueous alteration on IOM has been discussed by Orthous-Daunay et al. (2013) who concluded that there is no evidence of a low temperature oxidation alteration as proposed by Cody and Alexander (2005). The composition variations observed between CRs and Murchison or CIs (e.g. the

higher H/C ratio and alkyl abundance in CRs) has been attributed to pre-accretional heterogeneity. In the case of CM chondrites, the contribution of short duration thermal metamorphism has also been proposed, but the low number of CM chondrites investigated does not allow conclusions to be drawn on this contribution. Our new set of data shows that the most heavily altered chondrites (QUE 93005 2.1, Cold Bokkeveld 2.1) have chemically and structurally processed IOM. The IOM of mildly altered chondrites (Mighei 2.3, Nogoya 2.2, Murray 2.4/2.5) is characterized by a slight decrease of the CH₃/CH₂ ratio and Murchison 2.5 IOM is similar to CR IOM. Rubin (2012) has proposed that asteroidal collisions facilitates the extent of aqueous alteration in CM parent bodies. These collisions dissipate heat and Rubin (2012) proposed a link between short duration heating and the degree of aqueous alteration. The results presented here are both consistent with such an interpretation of the CM series and supported by shock experiments on bulk Murchison samples (Beck et al., 2011). In the case of Nogoya, Mighei and Murray, we infer that the collision was strong enough to slightly modify the CH₃/CH₂ ratio, but not enough to lead to detectable modifications of the structure and the abundance of other functional groups. The least aqueously altered chondrite studied here – Murchison – has the highest CH₃/CH₂ ratio. In this series of CMs, the most aqueously altered chondrites have the most thermally processed IOM. For most of these chondrites, including WIS 91600, the heating event was sufficiently mild or short in duration to preserve matrix hydration. Finally, both Tagish Lake and WIS 91600 have a Mg-rich mineralogy that points to a large extent of aqueous alteration (Fig. 1). They are also the most thermally processed chondrites according to IR and Raman data collected on IOM.

5.3 Radiogenic thermal metamorphism

The CR chondrites studied here, as well as the Murchison CM chondrite, do not show signatures of post-accretional thermal processing triggered by impacts. However, they have experienced low temperature and long duration thermal metamorphism controlled by radiogenic heating. The parent body temperatures measured for CI and CM chondrites range typically between 20 and 150 °C (Bullock et al., 2005; Guo and Eiler, 2007; Zolensky et al., 1991). For CR chondrites, estimations vary between 150 and 300 °C (Clayton and Mayeda, 1977; Weisberg et al., 1993). Using clumped carbonate thermometry, Guo and Eiler (2007) inferred temperatures in the range of 20-35 °C for Murchison and Murray and 71 °C for some Cold Bokkeveld samples. According to ⁵³Mn-⁵³Cr chronology, these temperatures were maintained over millions of years (Fujiya et al. 2013; de Leuw et al., 2009). Were such conditions favorable to the formation of IOM? In order to shed light on this discussion, we first address the case of sedimentary organic matter. Our goal is not to perform an irrelevant comparison, as the nature of the precursors and the maturation conditions are very different from those of chondritic IOM. However, in contrast with chondrites, the general context is much more constrained and the key parameters that control maturation are well identified.

Under terrestrial geological long duration conditions, kerogens (defined as the insoluble fraction of sedimentary organic matter) can form at low temperatures in sedimentary basins. Even at low temperatures that do not favor any chemical evolution on a laboratory time scale (< 1 yr), the formation of polyaromatic solids over thousands of years is possible. Numerous laboratory experiments and analysis of natural samples have demonstrated that an *organic precursor* exposed to thermal heating evolves through a so-called *carbonization process*, that involves the expulsion of hydrogen and heteroatoms (O, N, S...) and chemical evolution and structural transformation of the initial solid. The expelled molecular groups can be stabilized as free species if they migrate far enough from the heating source (depending on

the geology of the basins) or they may experience secondary carbonization (Barker, 1996; Behar et al., 2008). Several factors influence the carbonization rate and the composition/structure of the final residue. These include the nature of the precursor, temperature and time (Bostick et al., 1979; Waples, 1994; Barker, 1996), pressure, presence of water and confinement (Lewan et al., 1979; Michels et al. 1995). Different chemical models have been developed to predict the maturation of terrestrial kerogens (e.g. Barker, 1996; Behar et al., 2008 and references therein). The first-order parameters that control the maturation rate are the nature of the initial precursors and the time-temperature history (Vandenbroucke and Largeau, 2008). Thermal modeling of terrestrial kerogen maturation and laboratory experiments show that the maturation grade strongly depends on time, temperature and the nature of the organic precursors (Beny-Bassez and Rouzaud, 1985; Waples, 1994; Barker, 1996; Behar et al. 2008). The latter is quantified by a distribution of activation energies that describes parallel degradation reactions with different kinetics (Barker, 1996). Type I, II and III kerogens then appear significantly different in terms of their chemical evolution (Tissot et al. 1987).

In the case of chondrites, the temperatures determined correspond to specific conditions of formation or equilibration of carbonates, or to estimates derived from simple thermodynamic models with no kinetic treatment and that do not take into account the disordered character of some chondritic minerals (e.g. serpentines). In some cases, the temperatures are clearly overestimated, for instance for the CR chondrites (150-300 °C; Clayton and Mayeda, 1977; Weisberg et al., 1993). ^{53}Mn - ^{53}Cr chronology shows that aqueous alteration lasted several Ma, but no information on the time-temperature history is provided. Finally, most of the key parameters that control carbonization in natural conditions, i.e. the structure and composition of the organic precursor and the time-temperature history, appear to be largely unknown. *In this respect, existing knowledge on maturation processes in sedimentary basins on Earth is very helpful: the issue of IOM formation within a chondrite parent body is under-constrained. No reliable conclusions can be drawn.*

5.3 Organic precursors

The nature of the organic precursor must be considered when investigating the formation of chondritic IOM through thermal processing. A constraint is provided by IOM isotopic composition. The carbon and hydrogen isotopic compositions are heterogeneous at the molecular level. The most refractory (aromatic) part is depleted in D and ^{13}C , while the most volatile (aliphatic) part that cross-links the polyaromatic units is D and ^{13}C enriched (Mimura et al., 2005, 2007; Remusat et al., 2006; Okumura et al., 2011). Okumura et al. (2011) suggested that this observation supports the idea that IOM was formed from the assemblage of two components formed in ISM: (1) apolar aromatic species and (2) polar O-bearing chains. The D-enrichment has also been interpreted as ion-molecule reactions in the solar nebula subsequent to IOM formation (Remusat et al., 2006, 2010 and references therein). This statement may be inconsistent with the carbon isotopic composition as reported by Okumura et al., (2011), if both C and H fractionations are the result of the same chemistry. The ISM heritage described by Okumura et al. (2011) however raises questions. First, the size of the polyaromatic units in IOM is much smaller than the average size of the molecular species at the origin of the AIB bands (Tielens, 2008). This suggests that a process was at work to break these species in the protosolar disk. Second, a process is required to polymerize the different components and form a carbonaceous solid, which is not addressed by Okumura et al. (2011).

FT-ICR analysis of CH₃OH extractable soluble organic matter (SOM) has revealed a broad variety of molecules including polar O-bearing species (Schmitt-Koplin et al., 2009). The elemental composition of Murchison SOM was estimated to be $\sim C_{100}H_{155}O_{20}N_3S_3$. This composition differs from that of Murchison IOM ($\sim C_{100}H_{70}O_{18}N_3S_3$; Gardinier et al., 2000; Alexander et al., 2007) mostly with respect to the H content. In fact, carbonization may polymerize a complex mixture of molecules as found in SOM and may account for a cogenetic origin of SOM and IOM from the same organic precursor. Indeed, the secondary thermo-degradation of a kerogen produces products such as aliphatic chains or ether or carboxylic functional groups that crosslink polyaromatic units. Bitumens and petroleum oil are produced in terrestrial sediments by this mechanism (van Krevelen, 1993; Barker, 1996; VandenBroucke and Largeau, 2007). Therefore, we may infer that IOM and SOM are two byproducts of organic precursors that no longer exist in chondrites. These precursors were more hydrogen and oxygen-rich than SOM and IOM and could have been a mix of a broad variety of molecules produced at low temperatures, either in the dense core (Garrod et al., 2008) or the cold mid-plane of the protosolar disk. We may infer that they could be still present in the core of some cometary nuclei.

Finally, such a carbonization process must account for the isotopic composition of IOM, both in terms of the δD , $\delta^{15}N$ and $\delta^{13}C$ compositions and its heterogeneity at the molecular level. Unfortunately, we lack crucial information on the isotopic composition of the bulk SOM. For instance, the reported $\delta^{13}C$ compositions of small soluble molecules are positive, while $\delta^{13}C$ lies in the range [-35; -5 ‰] for IOM (Pizzarello et al., 2004; Alexander et al., 2007). However, the $\delta^{13}C$ composition of bulk SOM would be required to obtain a more meaningful comparison.

5.4 Ion irradiation as an alternative mechanism to thermal heating

An alternative mechanism to thermal processing is ion irradiation. Ion irradiation is known to be an efficient process to produce amorphous and disordered carbonaceous materials. Irradiation of icy films that contain a sufficient content of carbon atoms leads to amorphous carbons with a variety of polyaromatic structures that depend on irradiation conditions (Strazzula et al., 2001; Barrata et al., 2008). The polyaromatic structure of a carbonaceous material also evolves due to further irradiation. For instance, large polyaromatic units of soots of highly oriented pyrolyzed graphite can be broken, resulting in the broadening of G and D bands (Brunetto et al., 2009). Disordered carbons may also evolve toward a more amorphous solid, as testified by the disappearance of G and D peaks and the appearance of a broad single band peaking at 1500 cm⁻¹ (Strazzula et al., 2001). Another consequence of ion irradiation is the disappearance of the fluorescence background without narrowing the Raman G and D bands (Barrata et al., 2008). In contrast, thermal annealing decreases fluorescence but at the same time narrows the G and D bands. Interestingly, soot irradiation can produce carbon residue with Raman spectra very similar to those of the chondritic IOM (Brunetto et al., 2009). Finally, experimental studies demonstrated that irradiation generates disorder in carbonaceous material and that refractory carbonaceous materials can be formed from ices or mixtures of simple molecules. However, any experimental simulation could reproduce the polyaromatic structure of chondritic IOM. IOM formation by ion irradiation is a possibility that cannot be rejected, but dedicated experiments are required to thoroughly explore the settling of an IOM-like polyaromatic structure in various kinds of precursors.

5.5 Comparison with IDPs, AMMs and UCAMMs

IOM in IDPs, AMMs and UCAMMs (Ultra Carbonaceous AMMs) shows similarities with chondritic IOM, but has also significant differences with that of primitive chondrites. Raman spectra of IDPs, AMMs and UCAMMs are characterized by a large variation of the fluorescence background from negligible to very high values, preventing the detection of the carbon bands, and by larger variations in their Raman parameters (Fig. 15) (Wopenka, 1988; Quirico, et al. 2005; Bonal et al., 2006; Busemann et al., 2009; Dobrica, et al. 2011; Brunetto, et al. 2011; Bonal et al., 2011). Chemical variations between IDPs, AMMs, UCAMMs and carbonaceous chondrites have also been reported by XANES at C and N K-edges and by IR spectroscopy (Keller et al., 2004; Flynn et al., 2003; Dartois et al., 2013). This larger heterogeneity of the polyaromatic structure and chemical composition observed in stratospheric IDPs and in AMMs suggests more varying conditions during their formation. However, possible alteration processes during transit to Earth or in the Earth's atmosphere should also be considered. Heating and irradiation could have occurred during grain transit in the solar cavity that typically lasts around 10^4 years or by atmospheric flash heating or various oxidation processes during residence in the atmosphere or on the terrestrial ground (Rietmeijer, 1998; Munoz-Caro et al., 2006). Deciphering tertiary from primary (nebular) and secondary (parent body) chemical and structural features is not an easy task in this case. Dobrica et al. (2011) showed that sufficiently strong flash-heating leads to effects on IOM structure detectable in Raman spectra of scoriaceous AMMs by comparison with fine-grained AMMs. However, no firm conclusions can be drawn on possible heating effects on fine-grained AMMs.

On the other hand, a firm conclusion that can be drawn is that AMMs, UCAMMs and IDPs of cometary origin were definitely not thermally processed within their parent bodies. The IOM in cometary particles was clearly formed prior to accretion. Hence, comets are cold objects that are maintained at low temperature (< 30 K) for billions of years and are not heated above ~ 170 K during nucleus sublimation (Watanabe and Kouchi, 2008). The presence of liquid water within the nucleus is extremely unlikely, and if any, limited to scarce regions of the subsurface exposed to impacts. These upper conditions are consistent with the fact that a large fraction of stratospheric IDPs are olivine and pyroxene-rich, and present basically an anhydrous mineralogy (Rietmeijer, 1998). The primitive AMMs and UCAMMs sampled at CONCORDIA station also have an anhydrous mineralogy, consistent with a cometary origin (Dobrica et al., 2009). Therefore, IOM from IDPs, AMMs and UCAMMs was not formed through long duration thermal heating in their parent body as proposed by Cody et al. (2011). On the other hand, thermal processing may have occurred in the protosolar disk prior to accretion. Ion irradiation could have occurred either in the protosolar disk or within the subsurface of the cometary nucleus as suggested by Dartois et al. (2013).

6. CONCLUSION

We have performed an IR and Raman study of IOM in 27 primitive chondrites. Our main conclusions are the following:

1. According to their chemical composition (low CH_2/CH_3 ratio) and their polyaromatic structure, CR chondrites and possibly some CM chondrites such as Murchison are the chondrites that are processed the least by collision-induced metamorphism in their parent body or that have fully escaped short duration thermal metamorphism.

2. The degree of aqueous alteration of a CM chondrite increases with the amount of thermal processing of its IOM. This trend appears to be consistent with the observations of Rubin (2012) who suggested that aqueous alteration was facilitated by collisions.
3. Multi-wavelength Raman spectroscopy reveals that amorphous and disordered carbons formed in the laboratory by low temperature plasma condensation produces materials that are too disordered to reproduce the IOM structure without further heating of the samples.
4. Thermal processing may account for the production of both IOM and SOM through a thermo-degradation process as observed for kerogens within terrestrial sediment. Given the lack of knowledge on the nature of the precursor and the time-temperature history in the parent body, the location where this process took place cannot be firmly established. However, an alternative energetic process to thermal processing may be ion irradiation of the grains present in the protosolar disk prior to accretion or in the subsurface of the cometary nucleus as proposed in earlier studies.
5. Our data also confirm that IOM is structurally more homogeneous in chondrites than in stratospheric IDPs and AMMs. This may suggest that IOM contained in IDPs and AMMs was formed under more varying conditions. However, the effects of tertiary processes, such as atmospheric heating or irradiation during transit to Earth, may modify IOM structure. These effects need to be better understood before firm conclusions can be drawn.

ACKNOWLEDGEMENTS

This work has been funded by the Centre National d'Etudes Spatiales (CNES-France) and by the ANR COSMISME project grant ANR-2010-BLAN-0502 of the French Agence Nationale de la Recherche. We warmly thank the following institutes that provided us with precious meteorite samples: Meteorites Working Group (JSC Houston, USA), Museum National d'Histoire Naturelle (Paris, France), Smithsonian National Museum of Natural History (Washington DC, USA) and Naturhistorisches Museum (Vienna, Austria). We are very grateful to the three anonymous reviewers and to Sasha Krot (Assistant Editor) for providing very relevant comments that greatly improved the quality of the manuscript.

REFERENCES

- Abreu N.M. and Brearley A.J. (2010) Early solar system processes recorded in the matrices of two highly pristine CR3 carbonaceous chondrites, MET 00426 and QUE 99177. *Geochim. Cosmochim. Acta* **74**, 1146-1171.
- Abreu N.M. and Brearley A.J. (2008) Petrologic and chemical effects of the onset of aqueous alteration on the matrices in CR chondrites: GRA 95229. *Lunar and Planetary Science Conference Abstract* #2013.
- Aléon J., Robert F., Chaussidon M. and Marty B. (2003) Nitrogen isotopic composition of macromolecular organic matter in interplanetary dust particles. *Cosmochim. Geochim. Acta* **67**, 3773-3783
- Alexander C. M. O'D., Howard K. T., Bowden R. and Fogel M. L. (2013) The classification of CM and CR chondrites using bulk H, C and N abundances and isotopic compositions. *Geochim. Cosmochim. Acta* **123**, 244-260.
- Alexander C. M. O'D., Bowden R., Fogel M. L., Howard K. T., Herd C. D. K. and Nittler L. R. (2012) The provenance of asteroids, and their contributions to the volatile inventories of the terrestrial planets. *Science* **337**, 721-723.
- Alexander C. M. O. D., Fogel M., Yabuta H. and Cody G. D. (2007) The origin and evolution of chondrites recorded in the elemental and isotopic compositions of their macromolecular organic matter. *Geochim. et Cosmochim. Acta*. **71**, 4380-4403.
- Alexander C. M. O'D., Russell S. S., Arden J. W., Ash R. D., Grady M. M. and Pillinger C. T. (1998) The origin of chondritic macromolecular organic matter: a carbon and nitrogen isotope study. *Meteor. Planet. Sci.* **33**, 603-622.
- Barker (1996) Thermal modeling of petroleum generation: Theory and application. *Developments in petroleum science* 45. Ed. C. barker. Elsevier 512p.
- Barrata G. A., Brunetto R., Leto G., Palumbo M. E., SPinella F. and Strazzula G. (2008) Raman spectroscopy of ion-irradiated astrophysically relevant materials. *J. Raman Spec.* **39**, 211-219
- Beck P., Garenne A., Quirico E., Bonal L., Montes-Hernandez G., Moynier and Schmitt B. (2013) Transmission infrared spectra (2-25 microns) of carbonaceous chondrites (CI, CM, CV-CK, CR, C2-ungrouped): mineralogy, water, and asteroidal processes. Icarus, in press
- Beck P., De Andrade V., Orthous-Daunay F. R., Veronesi G., Cotte M., Quirico E. and Schmitt B. (2012) The redox state of iron in the matrix of CI, CM and metamorphosed CM chondrites by XANES spectroscopy. *Geochim. Cosmochim. Acta* **99**, 305-316
- Beck P., Yabuta H., Atou T., Quirico E., Yoldi-Martinez Z., Guillot A., Bonal L., Montagnac G., Schmitt B. and Montes-Hernandez G. (2011) Co-evolution of chondritic organics and minerals during impact metamorphism. *Lunar and Planetary Science Conference Abstract* #5331.

- Beck P., Quirico E., Montes-Hernandez G., Bonal L., Bollard J., Orthous-Daunay F.-R., Howard K.T., Schmitt B., Brissaud O., Deschamps F., Wunder B., and Guillot S. (2010) Hydrous mineralogy of CM and CI chondrites from infrared spectroscopy and their relationship with low albedo asteroids. *Geochim. Cosmochim. Acta* **74**, 4881-4892.
- Behar F., Lorant F. and Lewan M. (2008) Role of NSO compounds during primary cracking of a type II kerogen and a Type III lignite. *Org. geochem.* **39**, 1-22
- Bény-Bassez C. and Rouzaud J.-N. (1985) Characterization of carbonaceous materials by correlated electron and optical microscopy and Raman microspectroscopy. *Scanning Electron Microscopy* 119-132
- Bertrand P., Pittion J.L. and Bernaud C. (1986) Fluorescence of sedimentary organic matter in relation to its chemical composition. *Org. Geochem.* **10**, 641-647.
- Bonal L., Quirico E. and Bourot-Denise (2006) Determination of the petrologic type of CV3 chondrites by Raman spectroscopy of included organic matter. *Geochim. Cosmochim. Acta.* **70**, 1849-1863.
- Bonal, L., Bourot-Denise, M., Quirico, E., Montagnac, G., Lewin, E. (2007) Organic matter and metamorphic history in CO chondrites. *Geochim. Cosmochim. Acta* **71**, 1605-1623.
- Bonal L., Quirico E., Montagnac G. and Reynard B. (2006) Interplanetary dust particles: Organic matter studied by Raman spectroscopy and laser induced fluorescence. *Lunar and Planetary Science Conference*, Abstract #2271
- Bonal L., Quirico E. and Montagnac G. (2011). Structure of primitive polyaromatic carbonaceous matter: IDPs vs. Chondrites. *Met. Plan. Sci.* Abstract #5125
- Bonal L., Alexander C. M. O. D., Huss G. R., Nagashima K., Quirico E. and Beck P. (2013) Hydrogen isotopic composition of the water in CR chondrites. *Geochim. Cosmochim. Acta* In press.
- Bostick N., Cashman S., McCulloch T. & Waddell C. (1979) Gradients of vitrinite reflectance and present temperature in the Los Angeles and Ventura Basins, California. pp. 65-96 in: *Low-temperature Metamorphism of Kerogen and Clay Minerals* (D.F. Oltz, editor). Pacific Section, Society of Economic Paleontologists and Mineralogists, Los Angeles.
- Brownlee D. E. et al. (2006) Comet 81P/Wild 2 under a microscope. *Science* **314**, 1711-1716.
- Brunetto R., Pino T., Dartois E., Cao A-T, d'Hendecourt L., Strazzula G. and Brechignac P. (2009) Comparison of the Raman spectra of ion irradiated soot and collected extraterrestrial carbon. *Icarus* **200**, 323-337
- Brunetto R., Borg J., Dartois E., Rietmeijer F. J. M., Grossemy F., Sandt C., Le Sergeant D'Hendecourt L., Rotundi A., Dumas P., Djouadi Z., Jamme, F. (2011) Mid-IR, Far-IR,

Raman micro-spectroscopy, and FESEM-EDX study of IDP L2021C5: Clues to its origin. *Icarus* 212, 896-910.

Bullock E. S., Gounelle M., Lauretta D. S., Grady M. M. and Russell S. S. (2005) Mineralogy and texture of Fe-Ni sulfides in C11 chondrites: clues to the extent of aqueous alteration of the C11 parent body. *Geochim. Cosmochim. Acta* **69**, 2687-2700

Busemann H., Nguyen A. N., Cody G. D., Hoppe P., Kilcoyne A. L. D., Stroud R. M., Zega T. J. and L. R. Nittler (2009) Ultra-primitive interplanetary dust particles from the comet 26P/Grigg-Skjellerup dust stream collection. *Earth Planet. Sci. Lett.* **288**, 44-57.

Busemann H., Alexander C.M.O'D, and Nittler L.R. (2007) Characterization of insoluble organic matter in primitive meteorites by microRaman spectroscopy. *Met. Planet. Sci.* **42**, 1387-1416.

Clayton R.N. and Mayeda T.K. (1999) Oxygen isotope studies of carbonaceous chondrites. *Geochim. Cosmochim. Acta* **63**, 2089-2104.

Cody G. D., Heying E., Alexander C. M. O., Nittler L. R., Lilcoyne AL L. D., Sandford S. A and Stroud R. M. (2011) Establishing a molecular relationship between chondritic and cometary organic solids. *Proc. Nation. Acad. Sci.* **108**, 19171-19176

Cody, G. D. and Alexander, C. M. O. D. (2005) NMR studies of chemical structural variation of insoluble organic matter from different carbonaceous chondrite groups. *Geochim. Cosmochim. Acta.* **69**, 1085-1097.

Cronin J. R. and Chang S. (1993) Organic matter in meteorites: Molecular and isotopic analysis of the Murchison meteorite. In *The Chemistry of Life's Origins* (eds. C. X. Mendoza-Gomez, V. Pirronello, and J. Mayo Greenberg), Kluwer Academic Publishers, pp. 209-258.

Dartois, E., et al., 2007. IRAS 08572+3915: constraining the aromatic versus aliphatic content of interstellar HACs. *Astron. Astrophys.* **463**, 635-640

Dartois E., Marco O., Munoz-Caro G. M., Brooks K., Deboffle D. and d'Hendecourt L. (2004) Diffuse interstellar medium organic polymers. *Astron. Astrophys.* **423**, L33-L36.

De Leuw S. A. E. Rubin, A. K. Schmitt and J. T. Wasson (2009) ^{53}Mn - ^{53}Cr systematics of carbonates in CM chondrites: Implications for the timing and duration of aqueous alteration. *Geochim. Cosmochim. Acta* **73**, 7433-7442.

Derenne S., Rouzaud J-N, Clinard C. and Robert F. (2005) Size discontinuity between interstellar and chondritic aromatic structures: a high-resolution transmission electron microscopy study. *Geochim. Cosmochim. Acta* **69**, 3911-3918

Derenne S. and Robert F. (2010) Model of molecular structure of the insoluble organic matter isolated from Murchison meteorite. *Met. Plan. Sci.* **45**, 1461-1475

- Desert F-X., F. Boulanger and J. L. Puget (1990) Interstellar dust models for extinction and emission. *Astronom. Astrophys.* **237**, 215-236
- Dobrica, E., Engrand C., Duprat J., Gounelle M., Leroux H., Quirico E. and Rouzaud J.-N. (2009) Connection between micrometeorites and Wild 2 particles from Antarctic snow to cometary ices. *Met. Plan. Sci.* **44**, 1643-1661
- Dobrica E., Engrand C., Quirico E., Montagnac G. and Duprat J. (2011) Raman characterization of carbonaceous matter in CONCORDIA Antarctic micrometeorites. *Met. Planet. Spa. Sci.* **46**, 1363-1375.
- Ehrenfreund P., Robert F., d'Hendecourt L. and Behar F (1991) Comparison of interstellar and meteoritic organic-matter at 3.4 μm . *Astron. Astrophys.* **252**, 712-717.
- Endreß M. and Bischoff A. (1996) Carbonates in CI chondrites: Clues to parent body evolution. *Geochim. Cosmochim. Acta.* **60**, 489-507.
- Ferrari A. C. and Robertson J. (2001) Resonant Raman spectroscopy of disordered, amorphous, and diamondlike carbon. *Phys. Rev. B* **64**, 075414
- Ferrari A. C. and Robertson J. (2000) Interpretation of Raman spectra of disordered and amorphous carbon. *Phys. Rev. B* **61**, 14095
- Flynn G. J., Keller L. P., Feser M. Wirick S. and Jacobsen C. (2003) The origin of organic matter in the solar system: evidence from the interplanetary dust particles. *Geochim. Cosmochim. Acta.* **67**, 4791-4806.
- Fujiya W., N. Sugiura, Y. Sano and H. Hiyagon (2013) Mn-Cr ages of dolomites in CI chondrites and the Tagish Lake ungrouped carbonaceous chondrite. *Earth Planet. Sci. Lett.* **362**, 130-142.
- Gardinier A., Derenne S., Robert F., Behar F., Largeau C and Maquet J. (2000) Solid state CP/MAS C-13 NMR of the insoluble organic matter of the Orgueil and Murchison meteorites: Quantitative study. *Earth Planet. Sci. Lett.* **184**, 9-21.
- Garenne A., Beck P., Montes-Hernandez G., Quirico E., Bonal L., Schmitt B. and Chiriac R. (2012) Hydrogen abundance in carbonaceous chondrites from thermogravimetric analysis. *Mineralogical Magazine*, **76**, 1741
- Garrod R. T., Weaver S. L. W. and Herbst E. (2008) Complex chemistry in star-forming regions: an expanded gas-grain warm-up chemical model. *Ap. J.* **682**, 283-302.
- Godard M., Féraud G., Chabot M., Carpentier Y., Pino T., Brunetto R., Duprat J., Engrand C., Bréchnignac P., d'Hendecourt L. and Dartois E. (2012) Ion irradiation of carbonaceous interstellar analogues. Effects of cosmic rays on the 3.4 μm interstellar absorption band. *Astronom. Astrophys.* **529**, A146
- Gourier D., Robert F., Delpoux O., Binet L., Vezin H., Moissette A. and Derenne S. (2007) Extreme deuterium enrichment of organic radicals in the Orgueil meteorite: revisiting the interstellar interpretation ? *Geochim. Cosmochim. Acta* **72**, 1914-1923.

- Guo W. and Eiler J.M. (2007) Temperatures of aqueous alteration and evidence for methane generation on the parent bodies of the CM chondrites. *Geochim. Cosmochim. Acta* **71**, 5565-5575.
- Hayatsu R., Matsuoka S., Scott R. G., Studier M. H. and Anders E. (1977) Origin of organic matter in early solar system) VII. The organic polymer in carbonaceous chondrites. *Geochim. Cosmochim. Acta* **41**, 1325-1339
- Herd C. D. K., Blinova A., Simkus D. N., Huang Y., Tarozo R., Alexander C. M. M. O'D., Gyngard F., Nittler L. R., Cody G. D., Fogel M. L., Kebukawa Y., Kilcoyne A. L. D., Hiltz R. W., Slater G. F., Glavin D. P., Dworkin J. P., Callahan M. P., Elsilá J. E., De Gregorio B. T. and Stroud R. (2011) Origin and Evolution of Prebiotic Organic Matter As Inferred from the Tagish Lake Meteorite. *Science* **332**, 1304-1307.
- Kebukawa Y., Alexander C. M. O'D. and Cody G. D. (2011) Compositional diversity in insoluble organic matter in type 1, 2 and 3 chondrites as detected by infrared spectroscopy. *Geochim. Cosmochim. Acta*. **75**, 3530-3541.
- Kebukawa, Y., Nakashima S. and Zolensky M. E. (2010) Kinetics of organic matter degradation in the Murchison meteorite for the evaluation of parent-body temperature history. *Met. Planet. Sci.* **45**, 99-113.
- Keller L. P., Messenger S., Flynn G. J., Clemett S., Wirrick S. and Jacobsen C. (2004) The nature of molecular cloud material in interplanetary dust. *Geochim. Cosmochim. Acta*. **68**, 2577-2589.
- Kerridge J. F. (1999) Formation and processing of organics in the early solar system. *Space Sci. Rev.* **90**, 275-288.
- Kitajima F., Nakamura T., Takaoka N. and Murae T. (2002) Evaluating the thermal metamorphism of CM chondrites by using the pyrolytic behavior of carbonaceous macromolecular matter. *Geochim. Cosmochim. Acta* **66**, 163-172.
- Le Guillou C., Bernard S., Brearley A.J. and Remusat L. (2014) Evolution of organic matter in Orgueil Murchison and Renazzo during parent body aqueous alteration: In situ investigations. *Geochim. Cosmochim. Acta* In press
- Le Guillou C., Rouzaud J-N, Bonal L., Quirico E., Derenne S. and Remusat L. (2012) High resolution TEM of chondritic carbonaceous matter: Metamorphic evolution and heterogeneity. *Met. Plan. Sci.* **47**, 345-362
- Lewan M.D., Winters J.C. and McDonald, J.H. (1979) Generation of oil-like pyrolyzates from organic-rich shales. *Science* **203**, 897-899.
- Michels, R., Landais, P., Philp, R., Torkelson, B. (1994) Effects of pressure on organic matter maturation during confined pyrolysis of Woodford kerogen. *Energy Fuels* **8**, 741-754.
- Mimura K., Okamoto M., Nakatsuka T., Sugitani K. and Abe O. (2005) Shock-induced isotope evolution of hydrogen and carbon in meteorites. *Geophys. Res. Lett.* **32**, L11201.

- Mimura K., Okamoto M., Sugitani K. and Hashimoto S. (2007) Selective release of D and ^{13}C from insoluble organic matter of the Murchison meteorite by impact shock. *Meteor. Planet. Sci.* **42**, 347–355.
- Montes-Hernandez, G., Beck P., Pommerol A., Chiriack R., Brissaud O., Renard F., Yoldi-Martinez Z., Toche F., Moynier F., Quirico E., Schmitt B. and Bonal L. (2013) How much/many water in carbonaceous chondrites and hydrated asteroids? *Meteor. Planet. Sci.* In press
- Munoz-Caro G. M., Matrajt G., Dartois E., Nuevo M., d'Hendecourt L., Deboffle D., Montagnac G, Chauvin N., Boukari C. and Le Du D. (2006) Nature and evolution of the dominant carbonaceous matter in interplanetary dust particles: Effects of irradiation and identification with a type of amorphous carbon. *Astron. Astrophys.* **459**, 147-159.
- Naraoka H., Mita H., Komiya M., Yoneda S., Kojima H. and Shimoyama A. (2004) A chemical sequence of macromolecular organic matter in the CM chondrites. *Meteor. Planet. Sci.* **39**, 401–406.
- Okumura F. and Mumura K. (2011) Gradual and stepwise pyrolyses of insoluble organic matter from the Murchison météorite revealing chemical structure and isotopic distribution. *Geochim. Cosmochim. Acta* **75**, 7063-7080.
- Orthous-Daunay F.R., Quirico E., Beck P., Brissaud O., Dartois E., Pino T. and Schmitt B. (2013) Mid-infrared study of the molecular structure variability of insoluble organic matter from primitive chondrites. *Icarus* **223**, 534-543
- Orthous-Daunay F. R., Quirico E., Lemelle L., Beck P., deAndrade V. and Simionovi A. (2010) Speciation of sulfur in the insoluble organic matter from carbonaceous chondrites by XANES spectroscopy. *Earth Planet. Sci. Lett.* **300**, 321-328.
- Pendleton Y. J., Allamandola L. J. (2002) The organic refractory material in the diffuse interstellar medium: Mid-Infrared spectroscopy constraints. *Astrop. J.* **138**, 75-98
- Quirico, E., Bourot-Denise M., Robin C., Montagnac G. and Beck P. (2011) A reappraisal of the thermal history of EH3 and EL3 enstatite chondrites. *Geochim. Cosmochim. Acta* **75**, 3088-3102
- Quirico E., Montagnac G., Rouzaud J.-N., Bonal L., Bourot-Denise M., Duber S., and Reynard B. (2009) Precursor and metamorphic conditions effects on Raman spectra of poorly-ordered carbonaceous matter in chondrites and coals. *Earth Plan. Sci. Letters* **287**, 185-193.
- Quirico E., Montagnac G., Lees V., McMillan P. F., Szopa C., Cernogora G., Rouzaud J-N, Simon P., Bernard J-M, Coll P., Fray N., Minard R. D., Raulin F., Reynard B. and Schmitt B. (2008) New experimental constraints on composition and structure of tholins. *Icarus* **198**, 218-231.

- Quirico, E., Borg J., Raynal P-I, Montagnac G. and d'Hendecourt L. (2005a) A micro- Raman survey of 10 IDPs and 6 carbonaceous chondrites 2005. *Planet. Space. Sci.* **53**, 1443-1448.
- Quirico, E., Rouzaud J-N, Bonal L. and Montagnac G. (2005b) Maturation grade of coals as revealed by Raman spectroscopy: progress and problems. *Spectrochim. Acta A.* **61**, 2368-2377
- Quirico E., Raynal P. I. and Bourot-Denise M. (2003) Metamorphic grade of organic matter in six unequilibrated ordinary chondrites. *Meteor. Planet. Sci.* **38**, 795–811.
- Pizzarello S., Huang Y. and Fuller M. (2004) The carbon isotopic distribution of Murchison amino acids. *Geochim. Cosmochim. Acta* **68**, 4963-4969
- Raynal P.-I., Quirico E., Borg J., Deboffle D., Dumas P., d'Hendecourt L., Bibring J-P and Langevin Y. (2000) Using synchrotron infrared microscopy for the analysis of micronic extraterrestrial particules. *Planet. Space Sci.*, **48**, 1329-1339.
- Remusat L., Derenne S., Robert F. and Heike K. (2005a) New pyrolytic and spectroscopic data on Orgueil and Murchison insoluble organic: A different origin than soluble ? *Geochim. Cosmochim. Acta* **69**, 3919-3932
- Remusat L., Derenne S. and Robert F. (2005b) New insight on aliphatic linkages in the macromolecular organic fraction of Orgueil and Murchison meteorites through ruthenium tetroxide oxidation. *Geochim. Cosmochim. Acta* **69**, 4377-4386
- Remusat L., Palhol F., Robert F., Derenne S. and France-Lanord C. (2006) Enrichment of deuterium in insoluble organic matter from primitive meteorites: a solar system origin? *Earth Planet. Sci. Lett.* **243**, 15–25.
- Remusat L., Robert F., Meibom A., Mostefaoui S., Delpoux O., Binet L., Gourier D., and Derenne S. (2009) Protoplanetary chemistry recorded by D-rich organic radicals in carbonaceous chondrites. *Astrophys. J.* **698**, 2087–2092.
- Remusat, L., Guan Y. and Eiler J. M. (2010) Accretion and preservation of D-rich organic particles in carbonaceous chondrites: Evidence for important transport in the early Solar System nebula. *Astrophys. J.* **713**, 1048-1058.
- Rietmeijer F. J. M. (1998) Interplanetary Dust Particles. In *Planetary Materials, Reviews in Mineralogy* (ed. J. J. Papike). Mineralogical Society of America, Washington, DC **36**, 2-1 - 2-95
- Robert F. and Epstein S. (1982) The concentration and isotopic composition of hydrogen, carbon and nitrogen in carbonaceous meteorites. *Geochim. Cosmochim. Acta.* **46**, 81-95.
- Rouzaud J. and Oberlin A. (1990) Structure, microtexture, and optical properties of anthracène and saccharose-based carbons. *Carbon* **27**, 517–529.

- Rubin A. (2012) Collisional facilitation of aqueous alteration of CM and CV carbonaceous chondrites. *Geochim. Cosmochim. Acta* **90**, 181-194
- Rubin A. E., Trigo-Rodriguez J. M., Huber H. and Wasson J. T. (2007) Progressive aqueous alteration of CM carbonaceous chondrites. *Geochim. Cosmochim. Acta.* **71**, 2361-2382.
- Sandford S. A., Pendleton Y. J. and Allamandola L. J. (1995) The galactic distribution of aliphatic-hydrocarbons in the Diffuse Interstellar Medium. *Astrophys. J.* **440**, 697-705.
- Schmitt-Koplin P., Gabelica Z., Gougeon R.D., Fekete A., Kanawatu B., Harir M., Gebefuegi I., Eckel G., Hertkorn N. (2010) High molecular diversity of extraterrestrial organic matter in murchison meteorite revealed 40 years after its fall. *Proc. Nation. Acad. Sci.* **107**, 2763–2768.
- Strazzula G., Baratta G. A. and Palumbo M. E. (2001) Vibrational spectroscopy of ion-irradiated ices. *Spectrochim. Acta Part A* **57**, 825-842
- Tielens A. G. G. M. (2008) Interstellar polycyclic aromatic hydrocarbons. *Ann. Rev. Astron. Astrophys.* **46**, 289-337
- Tissot B.P., Pelet R. and Ungerer P. (1987) Thermal history of sedimentary basins, maturation indices, and kinetics of oil and gas generation. *AAPG Bulletin* **71**, 1445-1466
- Vandenbroucke M. and Largeau C. (2007) Kerogen origin, evolution and structure. *Org. Geochim.* **38**, 719-833.
- Van Krevelen, D. W (1993) *Coal. 3rd ed.; Elsevier: Amsterdam.*
- Wang M-S and Lipschutz M. E. (1998) Thermally metamorphosed carbonaceous chondrites from data for thermally mobile trace elements. *Meteor. Plan. Sci.* **33**, 1297-1302.
- Waples (1994) Maturity modeling: Thermal indicators, hydrocarbon generation, and oil cracking. In *The petroleum system-from source to trap: AAPG Memoir 60*. Maggon L. B. and W. G. Dow eds. 285-306
- Watanabe N. and Kouchi A. (2008) Ice surface reactions: a key to chemical evolution in space. *Prog. Surf. Sci.* **83**, 439-489
- Weisberg M.K., Prinz M., Clayton R.N., and Mayeda T.K. (1993) The CR (Renazzo-type) carbonaceous chondrite group and its implications. *Geochim. Cosmochim. Acta* **57**, 1567-1586.
- Wopenka B. (1988) Raman observations on individual interplanetary dust particules. *Earth Planet. Sci. Lett.* **88**, 221-231
- Yabuta H., Itoh S., Noguchi T., Sakamoto N., Hashiguchi M., Abe K., Tsujimoto S., Kilcoyne A.L.D., Okubo A., Okazaki R., Tachibana S., Terada K., Nakamura T. and Nagahara H. (2012). Coexisting nitrogen-rich and poor organic materials in ultracarbonaceous Antarctic micrometeorite. *Met. Plan. Sci.* Abstract #5196.

- Yabuta, H., Alexander C. M. O., Fogel M. L., Kilcoyne A. L. D. and Cody G. D. (2010). A molecular and isotopic study of the macromolecular organic matter of the ungrouped C2 WIS 91600 and its relationship to Tagish Lake and PCA 91008. *Met. Planet. Spa. Sci.* **45**, 1446-1460.
- Yabuta H., Naraoka H., Sakanishi K. and Kawashima H. (2005) Solid-state ^{13}C NMR characterization of insoluble organic matter from Antarctic CM2 chondrites: evaluation of the meteoritic alteration level. *Meteor. Planet. Sci.* **40**, 779–787.
- Yang, J. and Epstein S. (1983). Interstellar organic matter in meteorites. *Geochim. Cosmochim. Acta* **47**, 2199-2216.
- Zolensky M. E., Bourcier W. L., and Gooding J. L. (1989) Aqueous alteration on the hydrous asteroids: results of EQ3/6 computer simulations. *Icarus* **78**, 411-425.

Table 1: Sample classes and weathering and matrix hydration characteristics

	Class	Weathering category	Matrix hydration
Orgueil	CI	Fresh fall	H
Ivuna	CI	Fresh fall	H
Alais	CI	Fresh fall	H
EET 92042	CR2	B	H
GRA 95229	CR2	A	H
MET 00426	CR2	B	H
LAP 04516	CR2	B	n.d.
MAC 87320	CR2	Be	n.d.
PCA 91082	CR2	Be	n.d.
QUE 99177	CR2	Be	H
Renazzo	CR2	Fresh fall	H
GRO 95577	CR1	B	H
Mighei	CM >2.4 ¹	Fresh fall	H
Cold Bokkeveld	CM 2.2 ²	Fresh fall	H
Murchison	CM 2.5 ²	Fresh fall	H
Murray	CM 2.4/2.5 ²	Fresh fall	H
Nogoya	CM 2.2 ²	Fresh fall	H
QUE 97990	CM 2.6 ²	Be	H
QUE 99355	CM 2.3 ²	B	H
Banten	CM > 2.5 ¹	Fresh fall	n.d.
QUE 93005	CM 2.1 ²	A/Be	H
PCA 91008	CM2-heated	B	de-H
WIS 91600	CM2-heated	A/Be	de-H (largely)
Tagish Lake	C2-ung	Fresh fall	de-H (slightly)
Bells	C2-ung	Fresh fall	H
Essebi	C2-ung	Fresh fall	H
Acfer 094	C2-ung	strong	n.d.

[1] Ranked by IR microscopy. [2] From Rubin et al. (2007). H: hydrated. De-H: dehydrated. n.d.: not determined. Recommended types and weathering of Antarctic chondrites from the Meteoritical Bulletin Database.

Table 2: 514 nm Raman measurements on raw matrix grains

	Class	FWHM-G (cm ⁻¹)	ω (cm ⁻¹)	I _D /I _G	FWHM-D (cm ⁻¹)	ω (cm ⁻¹)
EET 92042	CR2	102.2 ± 4.0	1589.2 ± 1.9	0.89 ± 0.03	220.5 ± 9.4	1360.4 ± 1.9
GRA 95229	CR2	118.9 ± 7.5	1582.0 ± 3.6	0.83 ± 0.03	229.1 ± 7.7	1365.4 ± 4.4
MET 00426	CR2	102.0 ± 5.9	1591.8 ± 2.9	0.90 ± 0.03	219.9 ± 17.9	1362.9 ± 4.1
LAP 04516	CR2	101.9 ± 5.9	1592.4 ± 3.4	0.91 ± 0.06	220.9 ± 13.1	1362.8 ± 2.6
MAC 87320	CR2	106.0 ± 5.5	1590.0 ± 3.0	0.92 ± 0.05	223.9 ± 16.8	1363.9 ± 4.2
PCA 91082	CR2	101.2 ± 3.3	1591.4 ± 2.4	0.89 ± 0.04	214.4 ± 9.7	1363.4 ± 2.4
QUE 99177	CR2	102.8 ± 7.5	1590.0 ± 4.4	0.94 ± 0.07	217.8 ± 12.2	1364.0 ± 3.1
Renazzo	CR2	96.7 ± 7.1	1592.1 ± 3.0	0.93 ± 0.07	251.4 ± 15.1	1364.7 ± 3.4
QUE 95577	CR1	94.3 ± 3.0	1593.7 ± 1.6	0.90 ± 0.04	214.0 ± 7.9	1359.7 ± 2.1
Mighei	CM2	104.6 ± 3.2	1589.4 ± 2.2	0.90 ± 0.04	235.1 ± 7.9	1363.3 ± 2.0
Cold Bokkeveld	CM2.2	107.5 ± 3.8	1587.9 ± 1.9	0.87 ± 0.04	238.7 ± 13.9	1371.0 ± 3.6
Murray	CM2.4/2.5	107.0 ± 7.3	1587.4 ± 4.1	0.93 ± 0.07	226.7 ± 9.2	1362.6 ± 4.4
Nogoya	CM2.2	103.3 ± 5.8	1590.4 ± 3.0	0.92 ± 0.11	242.8 ± 14.2	1362.1 ± 2.1
QUE 97990	CM2.6	103.9 ± 6.5	1588.9 ± 3.7	0.91 ± 0.05	219.1 ± 5.6	1362.7 ± 3.0
QUE 99355	CM2.3	101.7 ± 2.4	1592.1 ± 1.6	0.97 ± 0.07	235.6 ± 9.7	1363.3 ± 2.5
Banten	CM2.?	107.6 ± 8.5	1588.4 ± 4.5	0.91 ± 0.05	224.3 ± 8.0	1363.8 ± 1.9
QUE 93005	CM2.1	81.7 ± 5.5	1596.9 ± 1.6	0.85 ± 0.06	237.7 ± 15.9	1363.6 ± 4.2
PCA 91008	CM2-heated	114.4 ± 4.8	1592.7 ± 3.6	1.10 ± 0.11	197.5 ± 12.9	1371.9 ± 4.9
WIS 91600	CM2-heated	99.5 ± 3.8	1594.4 ± 2.9	0.80 ± 0.03	237.4 ± 8.9	1366.8 ± 4.3
Tagish Lake	C2-ung	102.9 ± 5.6	1590.6 ± 3	0.80 ± 0.05	247.1 ± 10.3	1371.1 ± 4.1
Bells	C2-ung	111.4 ± 5.2	1584.3 ± 1.5	0.85 ± 0.05	253.9 ± 12.4	1364.7 ± 4.6
Essebi	C2-ung	111.3 ± 4.1	1584.2 ± 1.6	0.84 ± 0.06	252.0 ± 11.6	1365.1 ± 3.5
Acfer 094	C2-ung	103.0 ± 2.2	1589.1 ± 1.7	1.01 ± 0.02	210.5 ± 2.9	1359.9 ± 1.3

Table 3: 244 nm Raman measurements on IOM samples

	Class	FWHM-G (cm^{-1})	ω (cm^{-1})	I_D/I_G	FWHM-D (cm^{-1})	ω (cm^{-1})
Orgueil	CI	69.5 ± 1.8	1599.5 ± 3	0.19 ± 0.02	285.9 ± 6.2	1405.3 ± 4.3
Alais	CI	68.6 ± 1.8	1599.0 ± 3	0.18 ± 0.02	267.6 ± 7.7	1405.4 ± 4.4
Cold Bokkeveld	CM2.2	70.75 ± 1.6	1599.5 ± 3	0.21 ± 0.02	329.8 ± 24.9	1401.3 ± 7.8
Murchison	CM2.5	69.5 ± 2.8	1599.5 ± 3	0.17 ± 0.02	280.1 ± 16.2	1409.2 ± 5.4
PCA 91008	CM2-heated	78.0 ± 3.8	1614.75 ± 3	0.24 ± 0.06	276.4 ± 16.0	1427.8 ± 19.3
WIS 91600	CM2-heated	79.5 ± 2.0	1609.5 ± 3	0.24 ± 0.03	280.0 ± 14.1	1414.2 ± 6.8
Tagish Lake	C2-ung	70.5 ± 3.0	1603.5 ± 3	0.23 ± 0.02	303.7 ± 22.5	1409.2 ± 5.2

Table 4: Dispersion of the ω parameter

	Class	785 nm ω^1 (cm^{-1})	G-peak dispersion (cm^{-1}/nm)
Orgueil	CI	1594 ± 3	0.01
Alais	CI	1593 ± 3	0.01
MET 00426	CR2	1598 ± 3	0.02
Renazzo	CR2	1595.5 ± 3	0.01
Cold Bokkeveld	CM2.2	1594 ± 3	0.01-0.04
Murray	CM2.4/2.5	1594 ± 3	0.02
Nogoya	CM2.2	1593.5 ± 3	0.01
QUE 99355	CM2.3	1594 ± 3	0.01
QUE 93005	CM2.1	1593 ± 3	0.01
PCA 91008	CM2-heated	1603.5 ± 3	0.02-0.08
WIS 91600	CM2-heated	1586.5 ± 3	0.03-0.06
Tagish Lake	C2-ung	1585.5 ± 3	0.02-0.05

[1]: Measurements performed on IOM samples.

FIGURE CAPTIONS

Figure 1: Transmission infrared spectra of matrices of various chondrites. The band of variable width that peaks within $3690\text{-}3560\text{ cm}^{-1}$ suggests the presence of structural OH or molecular water in phyllosilicates or oxyhydroxides. The double-dotted vertical lines delimit the location of the peak of this band for the highly hydrated Orgueil (CI), the moderately altered QUE 97990 (CM2.6) and the weakly altered Renazzo (CR2) chondrites.

Figure 2: Untreated Raman spectra of CM and C2 ungrouped chondrites collected with a 514 nm excitation, showing broad G and D peaks superimposed on a fluorescence background of varying intensity. Metamorphosed CMs PCA 91008 and WIS 91600 display spectra almost devoid of fluorescence, as observed for type 3 chondrites (Bonal et al., 2006, 2007; Busemann et al., 2007). The “*” symbols indicate the signature of iron oxide(s).

Figure 3: Example of an LBWF fit performed on the Raman spectrum of the EET 92042 chondrite. The fluorescence background was previously subtracted assuming a linear baseline between 800 and 2000 cm^{-1} . The LBWF curve-fitting model does not provide a very good fit of the wing of the D band at low wavenumbers, and a misfit is also observed within the inter-band regions. Note that we did not use a free-floating baseline to improve the fit. The LBWF fit allows comparison with earlier studies of Ferrari and Robertson (2000, 2001). The results provided by this curve-fitting model for the chondrite series have been found to be consistent with those provided by principal component analysis.

Figure 4: The I_D/I_G parameter measured directly on reduced spectra against I_D/I_G derived from different curve-fitting models, for the 422 selected spectra of the 24 CR, CM and ungrouped-C2 chondrites. 2V: 2 Voigt profiles; 2L: 2 Lorentzian profiles; 2G: 2 Gaussian profiles; LBWF: Lorentzian Breit-Wigner-Fano profiles. The LBWF fit provides the best correlation.

Figure 5: Projections of the 422 spectra of the 24 CR, CM and ungrouped-C2 chondrites along the first two principal components plotted against the FWHM-G (top) and I_D/I_G spectral (bottom) parameters. Both these parameters account for a large fraction of the variance of the data set. Calculations were performed on a starting matrix of 422 lines (number of spectra) and 703 columns (Raman shift).

Figure 6: The Raman spectral parameters determined from the Lorentzian Breit-Wigner-Fano fit. Top (6a): FWHM-D vs. I_D/I_G . Middle (6b): FWHM-G vs. ω . Bottom (6c): ω vs. ω . Left: with guides for visual aid, without $1-\sigma$ error bars. Right: with $1-\sigma$ error bars. The orange group includes chondrites dissimilar to those of the main group, according to the I_D/I_G ratio or ω . See text for details.

Figure 7: Projections of the spectra along the first three principal components. Principal component analysis provided spectral differences similar to those obtained with the LBWF fit (see Fig. 6). Calculations were performed on a starting matrix of 422 lines (number of spectra) and 703 columns (Raman shift).

Figure 8: Comparison of the FWHM-G parameter (width of the G band) obtained in the present study with that obtained by Busemann et al. (2007).

Figure 9: FWHM-G plotted against O/C. The fairly good linear correlation suggests that oxygen heteroatoms play a key role in the cross-linking of polyaromatic units, possibly as ether bridges. It also suggests that the Raman measurements in the present study are reliable. O/C elemental ratios are from Alexander et al. (2007).

Figure 10: UV 244 nm Raman spectra collected on IOM extracted from different CI, CM and ungrouped C2 chondrites. The spectra are devoid of fluorescence background and display a narrow and intense G band along with a weak D band. The structure of IOM in PCA 91008 is very heterogeneous.

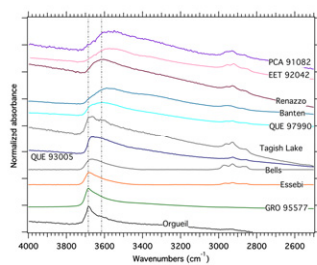
Figure 11: Raman spectral parameters extracted from 244 nm Raman spectra using an LBWF fit. The PCA 91008, WIS 91600 and Tagish Lake ungrouped C2 chondrites appear to be different than Orgueil, Ivuna and Murchison. The same is true for Cold Bokkeveld. These results are consistent with those obtained at 514 nm (Fig. 6).

Figure 12: Raw Raman spectra acquired with a red 785 nm excitation. The peak position of the G band was directly extracted from these raw spectra. Neither LBWF fitting nor principal component analysis was performed due to the lack of a reliable procedure to extract the fluorescence background.

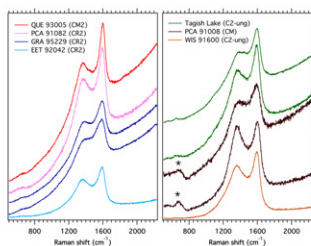
Figure 13: Infrared spectra of IOM extracted by HF/HCl protocol from CR and CM chondrites. The spectrum of the thermally processed WIS 91600 reveals lower aliphatic and carbonyl content than the unmetamorphosed GRA 95229, MET 00426, PCA 91082 (CR2) and Mighei (CM). The intriguing QUE 93005 (CM2.1) presents lower carbonyl content but a much larger abundance of alkyls.

Figure 14: Alkyl, CH₃/CH₂ ratio and C=O (carbonyl) relative abundances derived from IR spectra of IOM. The alkyl and C=O abundances are simply the integrated absorbance of the components used to fit spectra for which absorbance of the C=C peak was normalized to 1. The results can be displayed as 3 groups. Group I: no or undetectable parent body processing. Group II: short duration thermal metamorphism. Group III: mild parent body heating, detected by the CH₂/CH₃ ratio alone.

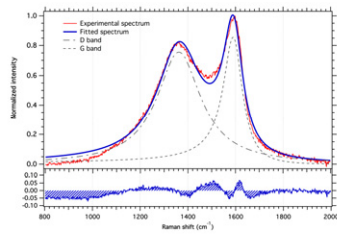
Figure 15: FWHM-G vs. ω plot (514 nm excitation) comparing chondritic IOM from this study, synthetic carbon materials from Ferrari et al. (2001) and coals from Quirico et al. (2003, 2005). The IOM polyaromatic structure is consistent with none of the carbon materials, except coals and ta-C:H annealed above 600 °C. Black arrows indicate the pathway of ta-C:H upon progressive annealing. These observations are confirmed by the ω dispersion calculated from Raman data acquired at the three excitation wavelengths (244, 514 and 785 nm).



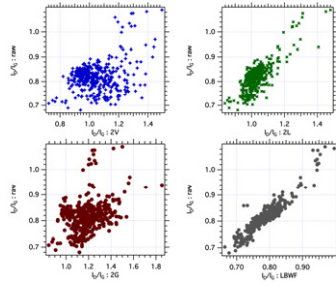
ACCEPTED MANUSCRIPT



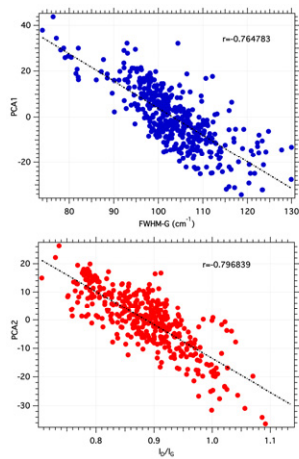
ACCEPTED MANUSCRIPT

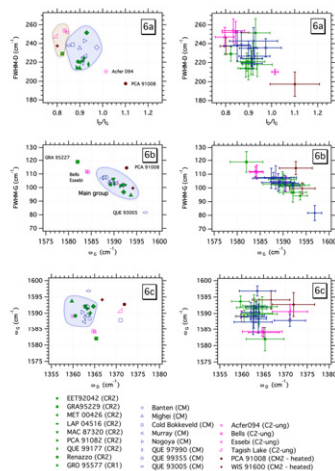


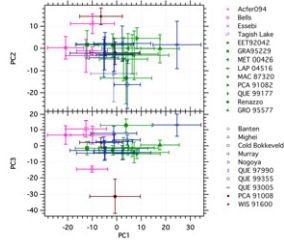
ACCEPTED MANUSCRIPT

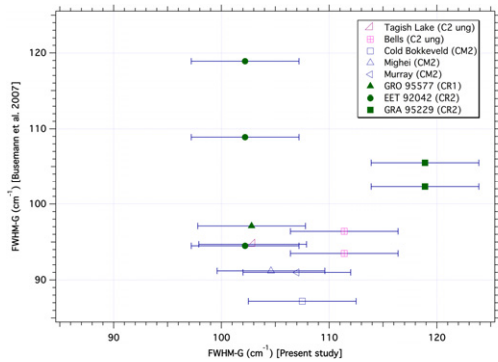


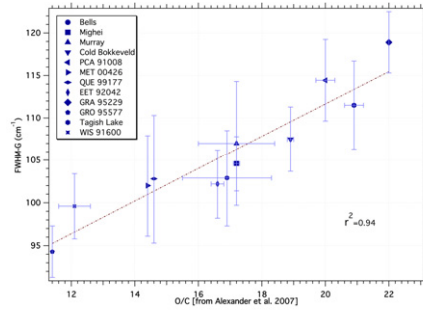
ACCEPTED MANUSCRIPT

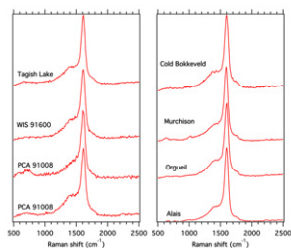




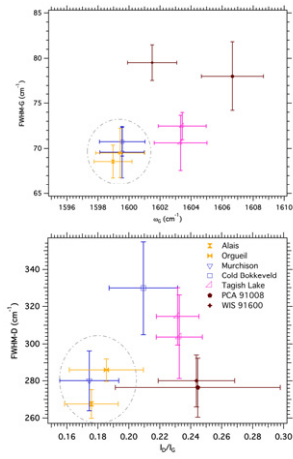


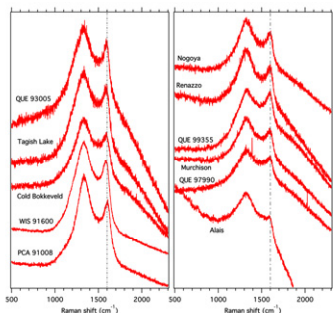




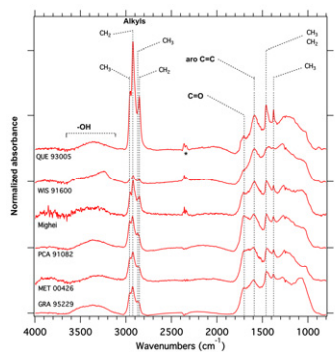


ACCEPTED MANUSCRIPT





ACCEPTED MANUSCRIPT



ACCEPTED MANUSCRIPT

